The Structure and Evolution of Unbound Star-forming Molecular Clouds

The Structure and Evolution of Unbound Star-forming Molecular Clouds

By

Rachel Louise Ward,

B.Sc. Spec. Hon., York University, 2009,

M.Sc., McMaster University, 2011

A Thesis

Submitted to the School of Graduate Studies

in Partial Fulfilment of the Requirements

for the Degree

Doctor of Philosophy

McMaster University

DOCTOR OF PHILOSOPHY (2015) McMaster University

(Department of Physics and Astronomy) Hamilton, Ontario

TITLE: The Structure and Evolution of Unbound Star-forming Molecular Clouds

AUTHOR: Rachel Ward, B.Sc. Spec. Hon., York University, 2009,
M.Sc., McMaster University, 2011

SUPERVISOR: Alison Sills & James Wadsley

NUMBER OF PAGES: xiv, 122

Abstract

Recent generations of stars form principally, and possibly exclusively, in giant molecular clouds – large conglomerations of gas and dust primarily composed of molecular hydrogen and concentrated in the arms of spiral galaxies. These clouds are assumed to be gravitationally bound; however, recent observations suggest the presence of a substantial population of unbound clouds in the Milky Way. Using synthetic observations from high-resolution simulations of bound and unbound molecular clouds, we explore whether clouds in this mixed population could match observations of local molecular clouds. We find from the clouds in our sample that a state of virial equilibrium is not required to form stars and match the dynamics and structure of observed clouds, as described by the Larson scaling relations and the probability distribution function (PDF) of the mass surface density. As these clouds evolve, the underlying lognormal shape of the column density PDFs is effectively concealed as the peaks of their distributions shift to surface densities below observational detection thresholds, supporting recent observations which also find little to no evidence for a lognormal distribution in column density PDFs of nearby clouds. We explore these results further in an extragalactic context by simulating molecular clouds formed in a galactic disc, in order to demonstrate the role their environment, particularly the galactic shear, plays on their structure and evolution and on the star formation within them. We find that a substantial population of unbound molecular clouds forms naturally in a galactic disc environment and demonstrate that their presence not only matches galactic and extragalactic observations but also impacts several long-standing issues in star formation.

Co-Authorship

Chapters 2, 3, and 4 of this thesis contain original scientific research written by myself, Rachel Louise Ward. Chapter 2 has been published as a peer-reviewed journal article in the Monthly Notices of the Royal Astronomical Society (MNRAS). The reference to this work is: *Ward, R. L., Wadsley, J., & Sills, A. 2014, MNRAS, Volume 439, Issue 1, pp. 651-658.* My co-supervisors, Dr. James Wadsley and Dr. Alison Sills, are the second and third authors. Chapter 3 has been published as a peer-reviewed journal article in MNRAS. The reference to this work is: *Ward, R. L., Wadsley, J., & Sills, A. 2014, MNRAS, Volume 445, Issue 2, pp.1575-1583.* Again, Dr. James Wadsley and Dr. Alison Sills are my co-supervisors and are the second and third authors, respectively. Chapter 4 has been submitted to MNRAS. The author list is as follows: *R. L. Ward, S. M. Benincasa, J. Wadsley, A. Sills, and H. M. P. Couchman.* My co-supervisors, Dr. James Wadsley and Dr. Alison Sills, are the third and fourth authors on this paper. Samantha Benincasa is the second author and she ran the galactic disc simulations and her supervisors are Dr. James Wadsley and Dr. Hugh Couchman, the third and fifth authors, respectively. All previously published material has been reformatted to conform to the required thesis style. I hereby grant an irrevocable, non-exclusive license to McMaster University and the National Library of Canada to reproduce this material as part of this thesis.

Acknowledgements

Hey everyone... remember how I said I would never get a Ph.D.?

I would like to begin by thanking my supervisors, Dr. Alison Sills and Dr. James Wadsley. Thank you for allowing me to pursue my dreams and walk my own path. Your guidance and insight have been incredibly valuable and have made this thesis all the better, resulting in a project of which I am immensely proud.

Many thanks also to my supervisory committee member, Dr. Christine Wilson, for your helpful advice and for offering a true observer's perspective on my research.

To all my office mates, past and present, and all of you who came through our revolving office door and were entertained by the "cultural and linguistic chaos" that is our office, there is light at the end of the tunnel and I never would have made it this far if it wasn't for you. Thank you for all the coffee runs, pancake breakfasts, office pranks, baking days, and softball games which left me with memories (and scars!) that will last a lifetime. You were always supportive and there to lend an ear... or a hand, often selflessly answering a desperate last-minute plea to help with a Let's Talk Science event. I especially want to thank Samantha Benincasa, who ran the galaxy disc simulations on which part of this work was based. Sam, we'll always have San Francisco!

I want to thank my friends and family who have supported me every step of this journey. To my parents, your unconditional love and support has carried me through some of the darkest moments. To know that you will always believe in me and be proud of me no matter what has given me the strength to see this through.

I decided to study astronomy because of two incredible mentors in my life: my high school science teacher, Sean Pedersen, and the director of the York University Observatory, Paul Delaney. Mr. Pedersen, your infectious enthusiasm, humour, and

passion for teaching made me love science and set me on this journey. I wish so very much that you could be here to read this, but know that you and your story will never be forgotten. Paul, until the day I met you I wasn't sure what I wanted to be "when I grow up." You were the one who convinced me to study astronomy and join the observatory team, instilling in me a life-long love of education and public outreach. Working for you at the observatory that first summer of my undergraduate degree also led to the most important moment of my life – the moment when a young A.J. Maxwell walked through your office door and said 'hello.'

Aaron, thank you for everything. You are my everything. You still – and will forever always – make my day.

Dedicated to the other Dr. R. Ward

"Happiness can be found, even in the darkest of times, if one only remembers to turn on the light."

Harry Potter and the Prisoner of Azkaban
Albus Percival Wulfric Brian Dumbledore (1881 - 1997)

"Real courage is when you know you're licked before you begin, but you begin anyway and see it through no matter what. You rarely win, but sometimes you do."

To Kill a Mockingbird
Harper Lee (1926 -)

"There will be a time when you believe everything is finished; that will be the beginning."

Louis L'Amour (1908 - 1988)

Table of Contents

List of Figures

List of Tables

Chapter 1

Introduction

Star formation is one of the most important physical processes in astrophysics. The formation of a single star can have far-reaching impact on the structure and evolution of its parent galaxy. It creates the seeds of future planets, enriches the galactic environment with the building blocks of life, and provides the energy necessary to sustain that life. Therefore, studying star formation feeds into all other areas of astrophysics, as it is inextricably linked to the formation of planets, evolution of galaxies, and the origin of life in the Universe.

Stars are born in large interstellar clouds – cold and dark nurseries composed of a filamentary web-like structure of gas and dust. These clouds typically reach masses of order a million Suns and span sizes tens of lightyears across. They have average densities of approximately 100 atoms cm^{-3} and are some of the coldest astronomical objects at a temperature only ten degrees above absolute zero. At these temperatures and densities, most of the gas is in the form of molecules, primarily molecular hydrogen, as the column density is high enough ($\sim 10^{21}$ atoms cm^{-2}) to self-shield against ultraviolet (UV) ra-

diation from nearby massive stars, which would otherwise cause the molecules to dissociate. These giant molecular clouds, or GMCs, are surrounded by the interstellar medium (ISM), which is the diffuse gas found between stars, and live predominantly in the spiral arm features of galactic discs. Understanding the nature of these clouds is important as it leads to a greater understanding of how they influence, and are influenced by, star formation and shape the structure and evolution of our own galaxy, the Milky Way.

Studying molecular clouds and star formation in detail is a challenge for many reasons. Stars form in the densest regions of molecular clouds called cores ($> 10^6$ atoms cm^{-3}) which are undergoing localised gravitational collapse, and are thus heavily obscured by the surrounding gas and dust. As a result, clouds appear opaque in observations at optical wavelengths. In order to probe the internal structure and dynamics of molecular clouds and reveal the properties of protostellar objects that form within them, infrared (IR), sub-millimetre, and radio observations are often used, as clouds are transparent at these longer wavelengths. Figure 1.1 demonstrates this increasing transparency with increasing wavelength for Bok Globule Barnard 68, a nearby compact dark cloud.

Also, although molecular hydrogen (H_2) is the most dominant molecule present in molecular clouds and is ubiquitous throughout the Galaxy, it is not directly observable (Kennicutt & Evans, 2012). Fortunately, H_2 can be traced by dust, such as in thermal continuum observations (e.g. Schlegel et al., 1998; Schnee et al., 2005; Lombardi et al., 2014) or extinction-based observations (e.g. Lada et al., 1994; Cambrésy, 1999; Lombardi & Alves, 2001; Lombardi,

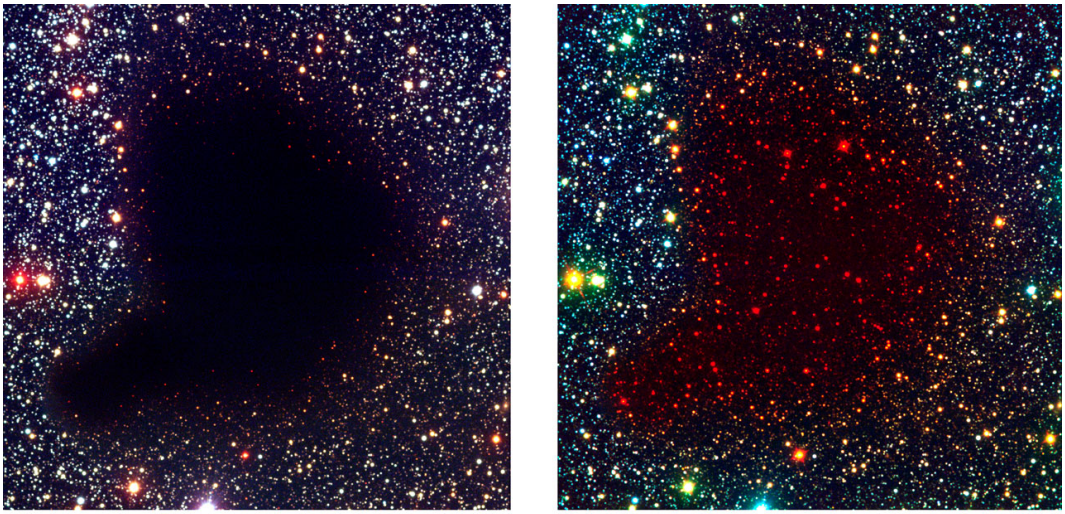

Figure 1.1 Bok globule Barnard 68 shown as a colour composite of optical (B, V) and near-infrared (I) wavelengths (left) compared to a colour composite of optical (B), near-infrared (I), and infrared (K) wavelengths (right). In the optical image ($V = 0.55$ μm), the cloud is opaque, but in the infrared image ($K = 2.16$ μm), it appears completely transparent. *Image credit: ESO.*

2009), or by using line emission from molecular tracers like carbon monoxide (^{12}CO) and its isotopologues (e.g. Solomon et al., 1987; Heyer et al., 2009).

As dust grains are heated by the interstellar radiation field, the resultant emission from the grains is re-radiated at far-infrared wavelengths. Using measurements of the flux at two far-IR wavelengths, the optical depth and temperature of the dust are determined by fitting the spectral energy distribution of the dust to a modified blackbody spectrum. Column density maps derived from these measurements of thermal dust emission rely on assumptions regarding the dust temperature distribution, opacities, and dust-to-gas mass ratio, causing them to be less reliable than other methods (Goodman et al., 2009; Lombardi et al., 2014).

Extinction maps are produced by measuring the absorption of light from background stars by intervening dust along the line of sight. Dust extinction can be measured using star counts to compare local stellar densities (e.g. Cambrésy, 1999) or by calculating the infrared colour excess, where the reddened spectra of the stars are compared to those for stars unaffected by dust, provided that the intrinsic colour of the background stars is known (e.g. Lada et al., 1994). The dust extinction, A_V, is typically measured in visual (V-band) magnitudes or in near-infrared wavelengths using K band-pass filters (A_K). The total dust extinction is then related to the H_2 mass surface density by assuming a conversion factor of

$$\Sigma / A_V = 20 \text{ M}_\odot \text{ pc}^{-2} \text{ mag}^{-1} \tag{1.1}$$

(Bohlin et al., 1978; Rieke & Lebofsky, 1985; Lombardi et al., 2010; Kainulainen et al., 2011; Lombardi et al., 2014). Extinction maps are useful for studying molecular clouds as they are affected by fewer uncertainties than spectral-line observations and have a larger dynamic range of surface densities (Goodman et al., 2009). These factors make extinction maps more suitable for studying the distribution of the gas in molecular clouds, which spans many orders of magnitude in density.

Alternatively, spectral-line observations typically have higher spatial resolution and less background noise than extinction maps. The spectral-line observations also provide an analogue to the third spatial dimension for an otherwise projected image on the sky by tracing the motion of the gas towards or away from us along the line-of-sight. These observations are made by measuring the emission from molecular tracers of H_2, such as the rotational line transitions of CO species (Pineda et al., 2008). These transitions occur at

densities between 10^{2-4} atoms cm^{-3} and certain isotopologues, like ^{13}CO, are optically thin, allowing emission at the full depth of the cloud to be detected, making CO an effective tracer for studying the dynamics of H_2 in molecular clouds.

In recent years, the premier telescope for the study of Galactic star formation has been the *Herschel Space Observatory* (Pilbratt et al., 2010), a space-based telescope sensitive in the far-infrared and submillimetre wavelengths, which achieved greater sensitivity and higher resolution than ever before. *Herschel* revealed that filaments, string-like chains of dense gas, are prevalent in molecular clouds and deeply embedded within these filaments are star-forming cores (e.g. André et al., 2010; Men'shchikov et al., 2010; Arzoumanian et al., 2011): a key result connecting the structure of molecular clouds to the process of star formation. Figure 1.2 shows an example of star formation occurring in a dense filament of the Taurus Molecular Cloud, observed in submillimetre wavelengths and combined with a background visible-light image of the star field in that region. The successor to *Herschel* is the ground-based *Atacama Large Millimetre Array* (ALMA), an interferometer of radio telescopes, which is unmatched in its spatial and spectral resolution and is poised to shed even more light on the formation of stars and planets throughout the coming years.

While detailed observations have been made of the internal structure of molecular clouds and newly-forming stars in our own Galaxy, these types of high-resolution studies in extragalactic observations of molecular clouds are currently impossible. Observations of nearby galaxies typically have cloud-scale resolution, limiting the ability to study extragalactic cloud properties in detail. This challenge can be partially overcome by combining data from

Figure 1.2 Star-forming cores deeply embedded in a filament in the Taurus Molecular Cloud observed using the APEX telescope, a pathfinder for ALMA. The submillimetre-wavelength observations are combined with a visible-light image of the star field in the region. *Image credit: ESO/APEX (MPIfR/ESO/OSO)/A. Hacar et al./Digitized Sky Survey 2. Acknowledgment: Davide De Martin.*

different surveys across multiple wavelengths. The advantage to observing in multiple wavelengths is that certain instruments can be used to achieve greater sensitivity and resolution while others are more sensitive at tracing different elements of the gas, dust, and stars. Recent studies using multi-wavelength observations (e.g. Rosolowsky et al., 2007; Bigiel et al., 2008, 2010a; Schinnerer et al., 2013) have succeeded at producing fully-sampled maps at high resolution, enabling the exploration of the relationship between the ISM, molecular clouds, and stars in nearby galaxies.

One drawback of observations is that they provide only a snapshot of astronomical objects projected on the night sky at one moment in time. Computer simulations on the other hand are visualisations in space *and* time. If an ob-

servation is the picture and theory is the frame, then simulations informed by theory and observation make it possible to animate that picture and time travel to any point in its history. Simulations provide a full three-dimensional view of an astronomical object, as well as a means to study its origin and evolution by re-winding and fast-forwarding over millions of years of time. Numerical hydrodynamic simulations are often used for studying molecular clouds and star formation, exploring the effects of such factors as turbulence, gravity, energy feedback from stars, radiative transfer, and magnetic fields. Although these effects are all important for star formation, most simulations cannot explore these factors simultaneously due to current limitations of the methods and the computational expense. While particle-based codes conserve physical quantities, have self-adaptive resolution, and have large dynamic ranges well-suited for systems where gravity plays a dominant role, they are less effective at capturing shocks and the effects of magnetic fields. Grid-based codes, on the other hand, can be used to model magnetohydrodynamic turbulence in addition to other physical processes, but do not always conserve energy and angular momentum and are not Galilean invariant (Bodenheimer et al., 2007). Often, simulators will use reduced physics to focus on the most dominant processes for the scale of interest, which harnesses the power of simulations while minimizing the various drawbacks. Comparing simulations to observations offers insight into which physical mechanisms play a dominant role in molecular clouds for a given scale.

Many simulators (e.g. Smith et al., 2008; Offner et al., 2009; Ward et al., 2012; Beaumont et al., 2013) have begun using synthetic observations to interpret their results, as they allow for a more direct comparison between sim-

ulations and observations. By studying simulations as though they are two-dimensional projections with a limited dynamic range, the simulations can be understood in the context of observations. Synthetic observations also demonstrate how various observational biases, such as background noise, projection effects, and assumptions regarding the gas-to-dust or CO-to-H_2 ratios, can have an effect on the accurate determination of cloud properties.

Studies involving molecular cloud simulations can typically be divided into two main categories: isolated cloud simulations and galactic disc simulations. The former allows the internal structure of the cloud and the evolution of that structure to be explored in great detail at high resolution (e.g. Bate et al., 2003; Tilley & Pudritz, 2004; Clark et al., 2005, 2008; Smith et al., 2008; Bate, 2009; Offner et al., 2009; Bonnell et al., 2011; Ward et al., 2012), where the latter focusses on the broader aspects of the molecular cloud population as a whole, such as their formation, the bulk properties of the clouds, their interactions with the disc and with one another, and the galactic star formation rate (e.g. Tasker & Tan, 2009; Tasker, 2011; Dobbs et al., 2011; Hopkins et al., 2011, 2012; Van Loo et al., 2013; Benincasa et al., 2013).

One open question surrounding star formation is with regards to rates and efficiencies in galaxies like the Milky Way. The expected star formation rate of a galaxy can be determined using estimates of the total molecular gas mass and the free-fall time ($t_{\rm ff}$) for collapse due to gravity given by

$$t_{\rm ff} = \sqrt{3\pi/32G\rho}, \tag{1.2}$$

where ρ is the average molecular gas density of the disc. Given that the molecular gas mass of the Milky Way is approximately 10^9 $M_\odot$ (Solomon et al., 1987), and the free-fall time is approximately 5 Myr, the expected

galactic star formation rate is approximately 200 $M_\odot$ yr^{-1}. However, the observed global star formation rate in the Milky Way is only 1 – 2 $M_\odot$ yr^{-1} (McKee & Williams, 1997; Robitaille & Whitney, 2010). This observed rate is significantly lower than expected, resulting in a very low star formation efficiency of ~ 1 %. Inefficient star formation is not limited to the Milky Way alone, as low galactic star formation rates and efficiencies are also observed in other galaxies (Kennicutt, 1998).

What is preventing these molecular clouds from collapsing to form stars? Magnetic pressure support was once thought to be the primary mechanism slowing the star formation process (e.g. Mouschovias, 1976), but recent studies (e.g. Mac Low & Klessen, 2004; Krumholz & McKee, 2005) argue more in favour of pressure support from supersonic turbulence. Some authors (e.g. Padoan & Nordlund, 2011; Federrath & Klessen, 2012) consider a combination of these factors to be necessary to explain the low star formation rate seen in observations. Stellar feedback from massive stars can also self-regulate star formation as energy injected from radiation pressure, stellar winds, and supernovae can disrupt molecular clouds, causing their dispersal (Hopkins et al., 2011). However, the most direct explanation for the low star formation rates observed is that a significant fraction of molecular clouds are gravitationally unbound (e.g. Clark & Bonnell, 2004; Clark et al., 2005).

An unbound molecular cloud has kinetic energy, K, from random motions of the gas that is greater than its gravitational potential energy, U, preventing it from collapsing on free-fall timescales and naturally producing a low rate and efficiency of star formation. By their nature, unbound molecular clouds are highly turbulent, transient objects and are easily prone to disruption. How-

ever, molecular clouds are typically assumed to be gravitationally bound and in virial equilibrium, such that they satisfy the virial theorem,

$$-2K = U. \tag{1.3}$$

The virial state of a molecular cloud can also be described by its observational virial parameter, α, defined as

$$\alpha = \left| \frac{2K}{U} \right| = \frac{5\sigma_{\rm v}^2 R}{GM} \tag{1.4}$$

(e.g. Bertoldi & McKee, 1992), where $\sigma_{\rm v}$ is the one-dimensional line-of-sight velocity dispersion, R is the cloud radius, and M is the gas mass of the cloud. If $\alpha = 1$, then the molecular clouds are stable to collapse and in virial equilibrium (or 'virialised'), where clouds with $\alpha \leq 2$ are gravitationally bound. The assumption that all molecular clouds are virialised stems from the seminal work of Larson (1981) who found three empirical scaling relations, commonly referred to as Larson's laws, that link the mass, size, and velocity dispersion of molecular clouds. Using a sample of molecular clouds, Larson showed that the three-dimensional velocity dispersion, $\sigma_{\rm 3D}$, of a cloud scaled with its size, L, such that

$$\sigma_{\rm 3D} = 1.1\ L^{0.38}. \tag{1.5}$$

This size-linewidth relation was confirmed in a follow-up study by Solomon et al. (1987), who found that $\sigma_{\rm v} \propto R^{0.5}$. The observed size-linewidth relation is consistent with predictions of the scaling behaviour for regions with supersonic turbulence. Turbulence plays an important role in the physics of star formation. As previously discussed, turbulence can provide support against global gravitational collapse, but it is also the principal driver of compressions promoting density fluctuations and localised collapse within molecular clouds

(Ballesteros-Paredes et al., 2007). Larson also found a scaling relation between the average number density, n, and size of molecular clouds, where

$$n \propto L^{-1.1}, \tag{1.6}$$

concluding that the column density of molecular clouds, $N = nL$, is approximately constant, independent of cloud size. A direct consequence of these two relations is that molecular clouds are gravitationally bound and in virial equilibrium. As expected, Larson finds that all molecular clouds in his sample are in approximate virial balance. These three "laws" have been used to characterise molecular clouds for the past thirty years, but the relations were derived using the best observations of that time, which had limited resolution and sensitivity. Recent observations at higher resolution and larger dynamic range by Heyer et al. (2009) show that molecular clouds can span a range of column densities and that Larson's conclusion that clouds have a constant column density is largely due to an observational selection effect. These observations also suggest that many of the nearby low-mass molecular clouds studied are unbound, consistent with the results of recent simulations of molecular clouds formed in galactic discs (Dobbs et al., 2011; Hopkins et al., 2012). The presence of a substantial population of unbound clouds would have implications for several open questions in star formation, including the star formation efficiency, the lifetimes of molecular clouds (whether they are long- or short-lived objects), and the nature of clustered vs. isolated star formation. These findings cast doubt onto the fundamental nature of Larson's laws and whether they are appropriate to characterise the nature of molecular clouds.

In this thesis, we investigate the consequences of a significant population of unbound clouds formed both in isolation and in a galactic disc environment.

We explore the true nature of molecular clouds through the lens of their internal structure, dynamics, and evolution and determine how these properties are affected by the external effects of the environment. From isolated simulations of molecular clouds formed out of turbulent regions of the ISM, we produce synthetic column density maps to directly compare to observations. Since the structure of a molecular cloud is hierarchical, this structure is best characterised by the distribution of column density throughout the cloud. This probability distribution function, or PDF, for the column density has been shown in observations by Kainulainen et al. (2009) to have a lognormal shape for quiescent clouds, but exhibit a strong power-law tail at high column densities for those actively undergoing star-formation (see Figure 1.3). We explore whether the structure of a cloud described by its column density PDF is dependent on its boundedness. We also study how that structure evolves with time and the effect of observational biases and limitations on how cloud structure and evolution are interpreted.

Molecular cloud structure, dynamics, and evolution are not just affected by internal properties of the cloud; they are also affected by external factors such as external pressure from the surrounding ISM, feedback from nearby supernovae, cloud-cloud collisions, and shear effects from the rotation of the galaxy (e.g. Tasker & Tan, 2009; Dobbs et al., 2011). We seek to determine if and how these environmental factors affect the properties of a population of bound and unbound clouds formed in a galactic disc simulation. By comparing clouds formed in a galactic disc to clouds formed in isolation, we hope to understand the role of environment as well as the impact of resolution on observationally-derived properties of local and extragalactic molecular clouds.

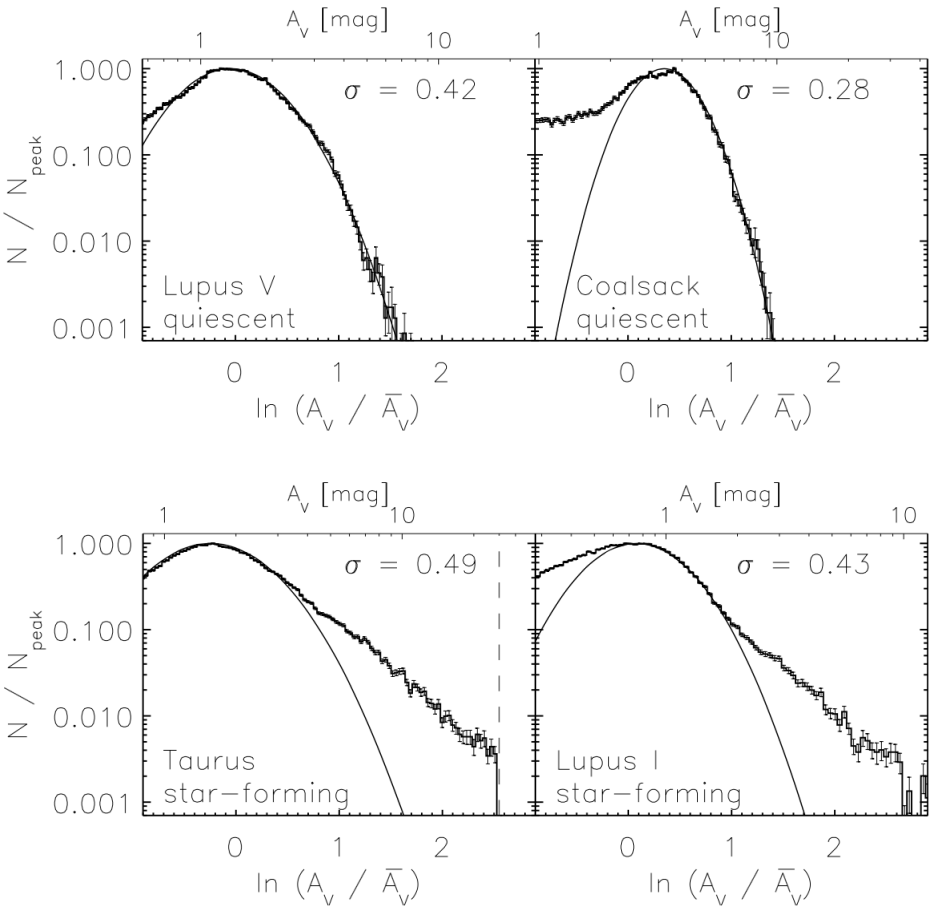

Figure 1.3 Probability distribution functions (PDF) of the column density for non-star-forming clouds Lupus V and Coalsack (top) and for actively star-forming clouds Taurus and Lupus I (bottom). The PDFs for these clouds are derived from near-infrared extinction (A_V) maps and normalized by the peaks of their distributions. The thin solid line shows the lognormal fit to each PDF, where σ is the width of the lognormal. *Image credit: Adapted from Figure 2 of Kainulainen, J. et al., 2009, "Probing the evolution of molecular cloud structure. From quiescence to birth," Astronomy and Astrophysics, Volume 508, Issue 3, pp.L35-L38. Reproduced with permission from Astronomy & Astrophysics,* © ESO.

This thesis is organized as follows. In Chapter 2, we use synthetic observations to study the dynamics of bound and unbound clouds and show that all clouds match observations and form star-forming cores regardless of whether or not they are bound or virialised. Using the same sample of bound and unbound clouds, we explore the evolution of structure in Chapter 3 and find that the peak of the lognormal column density PDF becomes undetectable as a cloud evolves, consistent with recent observations by Lombardi et al. (2014, 2015) and supporting the conclusion that clouds are transient objects with localised collapse into stars and global dispersal into the surrounding environment. In Chapter 4, we use synthetic observations of a simulated galaxy disc to study the statistical properties of molecular clouds in an extragalactic context. We find that clouds formed in the outer disc are smaller, lower mass clouds than those formed in the inner disc, which is a consequence of the weaker galactic shear rate at large galactocentric radii. We show that the rate of star formation within these clouds is also affected by the environment, particularly by the underlying surface density distribution of gas in the disc and the boundedness of their parent clouds. We close in Chapter 5 with a summary, the implications of our results, and discussion of future work.

Bibliography

André, P., Men'shchikov, A., Bontemps, S., et al. 2010, A&A, 518, L102

Arzoumanian, D., André, P., Didelon, P., et al. 2011, A&A, 529, L6

Ballesteros-Paredes, J., Klessen, R. S., Mac Low, M.-M., & Vazquez-Semadeni, E. 2007, Protostars and Planets V, 63

Bate, M. R., Bonnell, I. A., & Bromm, V. 2003, MNRAS, 339, 577

Bate, M. R. 2009, MNRAS, 392, 590

Beaumont, C. N., Offner, S. S. R., Shetty, R., Glover, S. C. O., & Goodman, A. A. 2013, ApJ, 777, 173

Benincasa, S. M., Tasker, E. J., Pudritz, R. E., & Wadsley, J. 2013, ApJ, 776, 23

Bertoldi F. & McKee C. F. 1992, ApJ, 395, 140

Bigiel, F., Leroy, A., Walter, F., et al. 2008, AJ, 136, 2846

Bigiel, F., Leroy, A., Walter, F., Blitz, L., Brinks, E., de Blok, W. J. G., & Madore, B. 2010a, AJ, 140, 1194

Bodenheimer, P., Laughlin, G. P., Rózyczka, M., & Yorke, H. W. 2007, *Numerical Methods in Astrophysics: An Introduction*, (New York: Taylor & Francis Group)

Bohlin, R. C., Savage, B. D., & Drake, J. F. 1978, ApJ, 224, 132

Bolatto, A. D., Leroy, A. K., Rosolowsky, E., Walter, F., & Blitz, L. 2008, ApJ, 686, 948

Bonnell, I. A., Bate, M. R., & Vine, S. G. 2003, MNRAS, 343, 413

Bonnell, I. A., Smith, R. J., Clark, P. C., & Bate, M. R. 2011, MNRAS, 410, 2339

Cambrésy, L. 1999, A&A, 345, 965

Clark, P. C., & Bonnell, I. A. 2004, MNRAS, 347, L36

Clark, P. C., Bonnell, I. A., Zinnecker, H., & Bate, M. R. 2005, MNRAS, 359, 809

Clark, P. C., Bonnell, I. A., & Klessen, R. S. 2008, MNRAS, 386, 3

Dobbs, C. L., Burkert, A., & Pringle, J. E. 2011, MNRAS, 413, 2935

Draine, B. T., & Li, A. 2001, ApJ, 551, 807

Federrath, C., & Klessen, R. S. 2012, ApJ, 761, 156

Goodman, A. A., Pineda, J. E., & Schnee, S. L. 2009, ApJ, 692, 91

Heyer, M. H., Carpenter, J. M., & Snell, R. L. 2001, ApJ, 551, 852

Heyer, M., Krawczyk, C., Duval, J., & Jackson, J. M. 2009, ApJ, 699, 1092

Hopkins, P. F., Quataert, E., & Murray, N. 2011, MNRAS, 417, 950

Hopkins, P. F., Quataert, E., & Murray, N. 2012, MNRAS, 421, 3488

Kainulainen, J., Lada, C. J., Rathborne, J. M., & Alves, J. F. 2009, A&A, 497, 399

Kainulainen, J., Beuther, H., Banerjee, R., Federrath, C., & Henning, T. 2011, A&A, 530, A64

Kennicutt, R. C., Jr. 1998, ApJ, 498, 541

Kennicutt, R. C., & Evans, N. J. 2012, ARA&A, 50, 531

Krumholz, M. R., & McKee, C. F. 2005, ApJ, 630, 250

Krumholz, M. R., & Tan, J. C. 2007, ApJ, 654, 304

Lada, C. J., Lada, E. A., Clemens, D. P., & Bally, J. 1994, ApJ, 429, 694

Larson, R. B. 1981, MNRAS, 194, 809

Lombardi, M., & Alves, J. 2001, A&A, 377, 1023

Lombardi, M. 2009, A&A, 493, 735

Lombardi, M., Alves, J., & Lada, C. J. 2010, A&A, 519, 7

Lombardi, M., Bouy, H., Alves, J., & Lada, C. J. 2014, A&A, 566, A45

Lombardi, M., Alves, J., & Lada, C. J. 2015, A&A, 576, L1

Mac Low, M.-M., & Klessen, R. S. 2004, Reviews of Modern Physics, 76, 125

McKee, C. F., & Williams, J. P. 1997, ApJ, 476, 144

Men'shchikov, A., André, P., Didelon, P., et al. 2010, A&A, 518, L103

Mouschovias, T. C. 1976, ApJ, 207, 141

Offner, S. S. R., Klein, R. I., McKee, C. F., & Krumholz, M. R. 2009, ApJ, 703, 131

Padoan, P., & Nordlund, Å. 2011, ApJ, 730, 40

Pilbratt, G. L., Riedinger, J. R., Passvogel, T., et al. 2010, A&A, 518, L1

Pineda, J. E., Caselli, P., & Goodman, A. A. 2008, ApJ, 679, 481

Rieke, G. H. & Lebofsky, M. J. 1985, ApJ, 288, 618

Robitaille, T. P., & Whitney, B. A. 2010, ApJL, 710, L11

Rosolowsky, E., Keto, E., Matsushita, S., & Willner, S. P. 2007, ApJ, 661, 830

Schinnerer, E., Meidt, S. E., Pety, J., et al. 2013, ApJ, 779, 42

Schlegel, D. J., Finkbeiner, D. P., & Davis, M. 1998, ApJ, 500, 525

Schnee, S. L., Ridge, N. A., Goodman, A. A., & Li, J. G. 2005, ApJ, 634, 442

Smith, R. J., Clark, P. C., & Bonnell, I. A. 2008, MNRAS, 391, 1091

Solomon, P. M., Rivolo, A. R., Barrett, J. & Yahil, A. 1987, ApJ, 319, 730

Tasker, E. J. & Tan, J. C. 2009, ApJ, 700, 358

Tasker, E. J. 2011, ApJ, 730, 11

Tilley, D. A., & Pudritz, R. E. 2004, MNRAS, 353, 769

Van Loo, S., Butler, M. J., & Tan, J. C. 2013, ApJ, 764, 36

Wadsley, J. W., Stadel, J., & Quinn, T. 2004, New Astronomy, 9, 137

Ward, R. L., Wadsley, J., Sills, A., & Petitclerc, N. 2012, ApJ, 756, 119

Chapter 2

Unbound Star-forming Molecular Clouds

Reprinted from Rachel L. Ward, James Wadsley, and Alison Sills, 2014, Monthly Notices of the Royal Astronomical Society*, Volume 439, Issue 1, pp. 651–658, DOI: 10.1093/mnras/stu004. Published by Oxford University Press on behalf of the Royal Astronomical Society.*

Abstract

We explore whether observed molecular clouds could include a substantial population of unbound clouds. Using simulations which include only turbulence and gravity, we are able to match observed relations and naturally reproduce the observed scatter in the cloud size-linewidth coefficient, at fixed surface density. We identify the source of this scatter as a spread in the intrinsic virial parameter. Thus these observational trends do not require that clouds exist in a state of dynamical equilibrium. We demonstrate that cloud virial parameters can be accurately determined observationally with an appropriate size estimator. All our simulated clouds eventually form collapsing cores, regardless of whether the cloud is bound overall. This supports the idea that molecular clouds do not have to be bound to form stars or to have observed properties like those of nearby low-mass clouds.

2.1 Introduction

Molecular clouds are the principal sites of star formation, as localised dense regions of gas and dust within a cold turbulent cloud collapse under gravity to form stars and stellar clusters. These highly supersonic clouds are typically tens of parsecs across, reaching masses of up to 10^6 $M_\odot$ in the Milky Way. In order to reach a greater understanding of how stars form and evolve, a logical first step is to explore the large-scale structure and dynamics of molecular clouds.

One approach is to characterise molecular clouds based on their large-scale properties: mass, size, and velocity dispersion. For the past thirty years, the three scaling relations presented in Larson (1981), commonly called Larson's Laws, have been used to link these properties. Larson found an empirical relation between the velocity dispersion and size of molecular clouds such that $\sigma_{3D} = 1.1\ L^{0.38}$ where σ_{3D} is the three-dimensional internal velocity dispersion in km s^{-1} and L is the maximum linear dimension in pc. Solomon et al. (1987) used a large sample of ^{12}CO observations of molecular clouds to find a similar size-linewidth relation of $\sigma_v = (1.0 \pm 0.1)\ S^{0.5}$ where σ_v is the one-dimensional velocity dispersion in km s^{-1} and S is a measure of the cloud size in pc. Although their results are consistent with Larson's, they do find a steeper power-law index of 0.5 which the authors argue is a consequence of clouds in virial equilibrium rather than due to a Kolmogorov turbulent spectrum, as suggested by Larson (1981). This interpretation by Solomon et al. (1987) is also consistent with Larson's second conclusion that molecular

clouds are gravitationally bound and in approximate virial equilibrium. The virial state of a cloud is often expressed using the virial parameter, α,

$$\alpha = \frac{5\sigma_{\rm v}^2 R}{GM}, \tag{2.1}$$

(e.g. Bertoldi & McKee, 1992) where $\sigma_{\rm v}$ is the one-dimensional velocity dispersion along the line of sight, R is the maximum projected radius, and M is the total mass of the cloud. The virial parameter describes simple virial equilibrium which excludes effects of magnetic fields and external pressure. Spherical, homogeneous clouds are virialised when $\alpha = 1$ and gravitationally bound if $\alpha \leq 2$. Larson's third scaling relation proposed that molecular clouds have approximately the same column density on all size scales; however, this conclusion was based on a sample with a limited range of column densities, which was the best achievable by observations at the time. If molecular clouds are assumed to be in gravitational equilibrium with a constant column density, then the size-linewidth relation naturally follows, implying the universality of molecular cloud structure and turbulence.

Although all three of Larson's scaling relationships are frequently used to define the characteristics of molecular clouds, there are often large amounts of scatter accompanying each trend, which varies in many cases by over two orders of magnitude (e.g. Larson, 1981; Heyer, Carpenter, & Snell, 2001; Ballesteros-Paredes et al., 2011; Wong et al., 2011). The scaling relations are often the focus of study while the scatter itself is readily dismissed. Whether this scatter is physically meaningful or a product of observational uncertainty is a subject which is explored throughout this work and also most notably in an influential study by Heyer et al. (2009) involving a re-examination of the Solomon et al. (1987) cloud sample using ^{13}CO observations with greater sensitivity and

higher spectral and angular resolution. Their results showed that the cloud column density is not constant, as confirmed in later studies (e.g. Kauffmann et al., 2010b; Lombardi et al., 2010; Ballesteros-Paredes et al., 2011), and that the scatter present in their size-linewidth relation is reduced when the scaling coefficient depends on the cloud mass surface density, Σ. The size-linewidth scaling coefficient, defined by Heyer et al. (2009) as

$$v_{\rm o} = \sigma_{\rm v}/R^{1/2} = (\pi G\Sigma/5)^{1/2}, \tag{2.2}$$

indicates that clouds inhabit a one-dimensional space parameterized by surface density. Heyer et al. (2009) suggested that the dependence of the size-linewidth coefficient, $v_{\rm o}$, on the surface density may not have been realized previously due to the limited range of column densities which could be probed in early observations of molecular clouds. The authors also note that scatter, while reduced, is still present in their data for the size-linewidth coefficient vs. the surface density.

A number of possible explanations for the cause of this remaining scatter have been proposed. Heyer et al. (2009) suggested that different interstellar magnetic field strengths and varying flux-to-mass ratios could produce the observed trend and scatter since the relation is consistent with models of magnetically-supported molecular clouds (Mouschovias, 1987). However, since the magnetic field strengths are unknown for this sample of molecular clouds, this cannot be confirmed by current observations. Alternatively, Field et al. (2011) found that the data of Heyer et al. (2009) can be accounted for by using different external pressure values for clouds in pressure-bounded virial equilibrium; however, the range of values necessary to reproduce the observed

trend extends much higher than current estimates for pressures present in the neutral ISM (Elmegreen, 1989; Bertoldi & McKee, 1992).

Ballesteros-Paredes et al. (2011) argue that neither magnetic support nor pressure confinement are required to explain the relation and scatter as the data are simply consistent with clouds undergoing hierarchical and chaotic gravitational collapse. Molecular clouds would have localised collapsing regions within a globally bound turbulent cloud, but these regions may not necessarily be virialised at all stages throughout their evolution. Although Heyer et al. (2009) find that most of the clouds in their sample are super-virial, they remark that their derived cloud masses could have been underestimated by a factor of 2 – 3. However, Dobbs et al. (2011) showed that even after doubling the cloud masses, most of the clouds in the Heyer et al. (2009) sample are not virialised with 50% of the clouds strictly unbound with $\alpha > 2$ in contrast to the common assumption of bound clouds.

The dependence of the size-linewidth coefficient on the mass surface density is expected from the definition of the virial parameter for clouds assumed to be gravitationally bound and virialised ($\alpha = 1$). However, there is considerable scatter present and the most direct interpretation of this scatter implies unbound clouds, $\alpha > 2$. Molecular clouds which are unbound as a whole can contain dense gravitationally bound subregions within them, such as clumps and cores, initially formed by supersonic turbulent motions and maintained by their own self-gravity. Whether or not molecular clouds can be truly unbound and still consistent with observations is the primary focus of this work.

Simulators have begun to explore the possibility that molecular clouds are unbound. Recent simulations (Clark et al., 2005, 2008; Bonnell et al., 2011)

have shown that unbound clouds can result in localised and distributed star formation and produce naturally low star formation efficiencies. Dobbs et al. (2011) explored the formation of molecular clouds through galaxy-scale simulations. Their simulated clouds were able to remain unbound, which the authors attributed to cloud-cloud collisions and stellar feedback. They produce molecular clouds with a wide range of virial parameters; however, they were not able to follow internal structure or dynamics in the clouds. Furthermore, their resolution prevents them from probing more typical cloud masses ($\lesssim 10^5$ $M_\odot$) such as those in the Heyer et al. (2009) sample.

Our simulations have been designed to avoid potential biases associated with assuming molecular clouds are initially bound, that they have a preferred surface density, or other assumptions that predispose them to collapse and star formation. We produced a set of 16 high resolution simulations, with properties listed in Table 2.1, that cover a broad range of initial column densities and turbulent velocities. Our simulations evolve to form local regions with surface densities typical of observed molecular clouds. Unlike most other studies, the clouds also contain large-scale turbulent motions so they do not collapse spherically. In this paper, we present properties of these clouds as they would be observed. To create a sample of synthetic observations at various stages of evolution, we selected localised dense turbulent regions analogous to low-mass clouds, such as the Taurus molecular cloud (1.5×10^4 $M_\odot$; Pineda et al., 2010) and the Perseus molecular cloud (7×10^3 $M_\odot$; Arce et al., 2010). We demonstrate the ability of these clouds to form stars, and we offer a simple explanation for the scatter present in the v_o-Σ relation.

In Section 2.2, we describe the details of our suite of simulations followed by a description of our cloud selection criteria and methods of analysis in Section 2.3. We present our results and explore the effect of boundedness on the determination of cloud properties in Section 2.4. Finally, we summarize our results in Section 2.5.

2.2 The Simulations

Using the smoothed particle hydrodynamics code, GASOLINE (Wadsley et al., 2004), we ran sixteen simulations of a 50 000 $M_\odot$ region of the ISM which include the effects of decaying initial turbulence and gravity. This allows us to study the dynamics and evolution of molecular clouds without the additional complications of magnetic fields, variable external pressure, or stellar feedback.

The simulations use the same equation of state and open boundary conditions as those described in Ward et al. (2012). Since our equation of state from Bate & Bonnell (2005) has an opacity limit for fragmentation of 10^{-13} g cm^{-3} much higher than our maximum gas density, our entire simulations are optically thin and isothermal at 10 K. Each run is simulated using approximately 5.5 million particles, resulting in one of the most massive and highly resolved simulations of an isolated cloud currently achieved, with a mass resolution of 8.85×10^{-3} $M_\odot$ per particle.

We used a Burgers' turbulent velocity spectrum characterised by three eigenvectors of the symmetric shear tensor, where material along one axis expanded outward, material along another axis collapsed inward, and the third dimension remained static. We refer to this type of anisotropic collapse as the

'ribbon' collapse case (Petitclerc, 2009; Ward, 2011), which was determined by Petitclerc (2009) through a statistical study of the anisotropy of cloud collapse to be the most likely scenario to be observed in nature, assuming that all molecular clouds have random turbulence on large-scales. Our simulations include turbulent modes larger than the scale of the cloud to account for large-scale effects. The resultant flow structure has some similarities with that of a cloud formed from a colliding flow. It also has a very filamentary structure which is in agreement with current observations of molecular clouds (e.g. Men'shchikov et al., 2010; Arzoumanian et al., 2011). In order to avoid the high computational costs of simulating such a large range of densities typical of observed clouds, the highest density regions ($> 10^6$ atoms cm^{-3}) were replaced by sink particles with the requirement that these regions were at a potential minimum and were gravitationally bound (cf. Federrath et al., 2010). The simulations are run until a maximum of 35% in mass of the gas is converted to stars. Since several of our runs are initially unbound, the mass fraction in stars is not directly coupled to the free-fall time, resulting in different absolute stopping times for each run. However, each simulation was run until $t = 0.5\ t_{\rm ff}$ at the very least, where $t_{\rm ff} = 1/\sqrt{G\rho_{\rm initial}}$.

The initial conditions of our simulations were chosen such as to have initial physical virial parameters ranging from $\alpha_{\rm initial} = 1$ (bound and virialised) to $\alpha_{\rm initial} = 10$ (highly unbound). This was achieved using a range of densities, $n_{\rm initial}$, and velocity dispersions, $\sigma_{\rm 3D}$, listed in Table 2.1, resulting in column densities between $1 - 7 \times 10^{21}$ cm^{-2}. For comparison, observed molecular clouds have a mean extinction of $A_{\rm v} \approx 1$ which corresponds to a column density of $\sim 10^{21}$ cm^{-2} (Bohlin et al., 1978). Although infrared dark clouds

Table 2.1 Initial Conditions for the Simulations

Id	Radius (pc)	σ_{3D} (km s^{-1})	$n_{initial}$ (cm^{-3})	t_{ff} (Myr)	$\alpha_{initial}$
1	30	6.56	7.69	22.4	10
2	21.2	7.80	21.8	13.3	10
3	15	9.27	61.5	7.9	10
4	10.6	11.0	174	4.7	10
5	30	4.39	7.69	22.4	4
6	21.2	5.22	21.8	13.3	4
7	15	6.20	61.5	7.9	4
8	10.6	7.38	174	4.7	4
9	30	2.93	7.69	22.4	2
10	21.2	3.49	21.8	13.3	2
11	15	4.15	61.5	7.9	2
12	10.6	4.93	174	4.7	2
13	30	2.07	7.69	22.4	1
14	21.2	2.47	21.8	13.3	1
15	15	2.93	61.5	7.9	1
16	10.6	3.49	174	4.7	1

can reach column densities of $\sim 10^{24}$ cm^{-2} (Ballesteros-Paredes et al., 2011), near-infrared dust extinction data for molecular clouds can only probe to a maximum column density of $\sim 25 \times 10^{21}$ cm^{-2} due to the observational limitations of this method (Kainulainen et al. (2009), and references therein).

Our simulations of the 50 000 M$_\odot$ region of the ISM evolve under gravity and turbulence to form molecular clouds with masses ranging from $\sim$ 300 to 10 000 M$_\odot$. Detailed properties of these clouds and the process by which they were selected are provided in Section 2.3.

2.3 The Cloud Selection Process

In order to compare the results of the simulations with observations, we have created a synthetic two-dimensional column density map for each of the sixteen cases using the method described in Ward et al. (2012). Our column density maps were produced from the simulation by interpolating the SPH particles to a 4000 × 4000 grid, where the spatial resolution is 6000 AU per pixel. The SPH kernel function (Monaghan & Lattanzio, 1985) is used to smooth each particle over several grid cells and is weighted to ensure normalization of the total mass in the map. A sample synthetic column density map is shown in Fig. 2.1a. We can assume that the column density of material in our maps is a direct analogue of extinction measurements or of the observed flux from ^{13}CO observations since our gas is optically thin for the duration of each simulation. The cloud sample was created by examining each simulation at 1 Myr intervals for a total of 122 snapshots. Individual clouds typically appear at around 1/4 of a free-fall time and sinks, representing a star or small groups of stars, begin to form at a similar time. The sample therefore represents molecular clouds at many different stages of evolution.

Fig. 2.1b demonstrates the method of cloud selection. We temporarily smoothed our maps to 1 pc spatial resolution using a Gaussian filter to emphasise the large-scale structure. This spatial resolution was chosen to be similar to the best resolution of the nearby molecular cloud observations by Solomon et al. (1987) and our selection process is intended to mimic theirs. The grey contour lines mark the minimum possible column density, $\sigma_{\rm th} \approx 0.5 \times 10^{21}$ cm^{-2}, that can be detected from dust extinction measurements (Kainulainen et al., 2009). To be considered a cloud, the extended emission

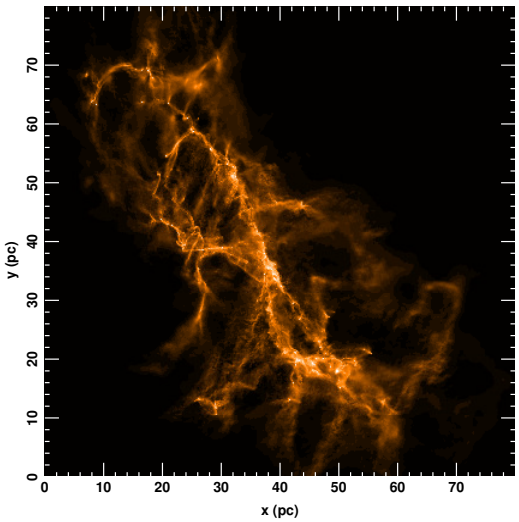

(a) Sample Map

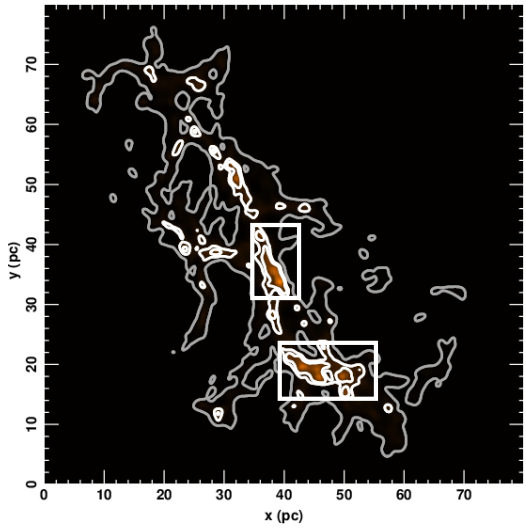

(b) Smoothed Contour Map

Figure 2.1 Sample synthetic column density maps for a marginally bound ($\alpha_{\rm init}$ = 2) case with an initial radius of approximately 21 pc at 0.6 $t_{\rm ff}$. The top figure shows the full range of column density we can cover in our simulation. The map has logarithmic scaling with a maximum column density of 25 $\times$ 10^{21} cm^{-2}. The figure on the bottom shows a map with a limited range of column density more consistent with observations. The minimum contour level for consideration to be selected as a cloud (white contour) is chosen to be three times the value of our chosen threshold, $\sigma_{\rm th}$ = 0.5 $\times$ 10^{21} cm^{-2} (grey contour). The boxes identify the two clouds in this map which meet the selection criteria outlined in the text.

above the white contour lines, which have a minimum threshold of $3\sigma_{\rm th}$ and contour intervals of $3\sigma_{\rm th}$, must be contiguous with box dimensions greater than 3 pc across, where the size threshold distinguishes clouds from smaller star-forming clumps (Bergin & Tafalla, 2007). These newly-identified clouds were extracted from the simulations using a box size defined by the contour threshold in order to isolate and study local regions within the simulations. This selection allows for a more direct comparison with clouds like the Taurus molecular cloud and the Pipe Nebula. Our entire sample includes 181 clouds with masses ranging between $100 - 10^4$ $M_\odot$, consistent with observed masses of nearby clouds (Kainulainen, Federrath, & Henning, 2013). Our population of clouds also spans a range of dynamical states, where some clouds are actively star-forming (localised collapse to densities greater than 10^6 cm^{-3}) and others are much more quiescent.

2.4 Results

2.4.1 Comparison to Observations

To ensure that the simulated molecular clouds are consistent with real molecular clouds, we compared properties determined from our synthetic column density maps to those measured in observations. For the clouds in our sample, we only included pixels above a minimum column density threshold of 0.5×10^{21} cm^{-2} in our determination of the mass, size, and linewidth. This column density threshold corresponds to the lower limit for detection in extinction maps ($A_{\rm v} \sim 0.5$; Bohlin et al., 1978) which also coincides with the

threshold for self-shielding against UV feedback leading to the formation of molecular clouds.

The cloud mass, M, is the total mass in the pixels above the threshold in each simulated cloud. Our cloud masses are consistent with those measured in observations of nearby clouds (median mass of nearby clouds = 5000 $M_\odot$; Kainulainen, Federrath, & Henning, 2013). We have excluded sink particles from our estimations since the effects of stars are not included in observational estimates of molecular cloud properties. Embedded stars bias measurements in extinction-based data due to pixel 'saturation' (see Goodman et al., 2009; Kainulainen et al., 2009), and in molecular line observations, the use of CO and its isotopologues as tracers of H_2 cause 'freeze-out' onto dust grains at densities of $\gtrsim 10^4$ cm^{-3}. Also, Kainulainen, Federrath, & Henning (2013) recently explored the effect of sink particles on the surrounding gas in their simulations of molecular clouds and argued in favour of their removal.

We determined the line-of-sight velocity dispersions, σ_{v_i}, using the mass-weighted velocities of the gas particles in our simulation, $\langle v_i \rangle$, such that $\sigma_{v_i}^2 = \langle v_i^2 \rangle - \langle v_i \rangle^2$. To avoid any dependence of the velocity dispersion on our single (arbitrarily chosen) line-of-sight, we used the averaged one-dimensional velocity dispersion to represent the linewidth:

$$\sigma_{\rm 1D} = \left(\frac{\sum_i \sigma_{v_i}^2}{3} \right)^{1/2}, \quad i = x, y, z. \tag{2.3}$$

The mass surface density is given by $\Sigma = M/\pi R^2$, where R is the radius of the cloud; however, the radius can be quite difficult to determine as cloud boundaries can be subjective and dependent on the interpretation of the observer. Molecular clouds are often first detected using CO observations (Wilson & Scoville, 1990; Lada et al., 2009), where the size is measured as

the full extent of molecular emission (Solomon et al., 1987). However, several authors argue that dust extinction maps are best for determining the spatial distribution of a cloud as they are affected by fewer uncertainties and can probe a larger dynamic range (Goodman et al., 2009; Kainulainen et al., 2009; Kauffmann et al., 2010a; Lombardi et al., 2010; Beaumont et al., 2012). To determine which is a more appropriate estimate of size, we compare two means of measuring the cloud area using our sample of simulated clouds.

We initially defined the area of our clouds using the same method of Solomon et al. (1987) and Heyer et al. (2009), who used an intensity-weighted size dispersion to determine the angular extent of each molecular cloud. As an analogy to intensity-weighting, we use the mass in each pixel to weight the size dispersions of our clouds, which are σ_x and σ_y in the x-y plane. To relate the size parameter, $S_{xy} = \sqrt{\sigma_x \sigma_y}$, to the projected area of the cloud, S_{xy} is scaled by a factor of 3.4 (Solomon et al., 1987), such that the effective radius, $R_{\rm S}$, is defined to be

$$R_{\rm S} = \frac{3.4}{\sqrt{\pi}} S_{xy}. \tag{2.4}$$

Fig. 2.2 shows the linewidth plotted as a function of radius as defined by Solomon et al. (1987), $R_{\rm S}$, for our clouds (black stars), as compared to real clouds (grey symbols) from the observations of Heyer et al. (2009). Heyer et al. (2009) use two methods of measuring area to determine their cloud properties: the primary area, A_1, defined by the boundaries used by Solomon et al. (1987) as described above and a secondary area, A_2, corresponding to the highest column density regions and defined by the area within the half-power isophote of the peak column density. Both data sets are included in Fig. 2.2 to demonstrate the range of size estimates made by observations. Our clouds

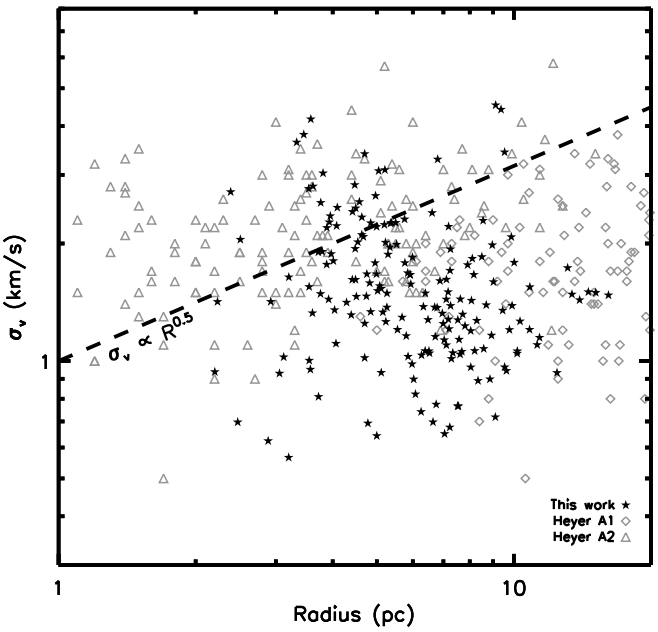

Figure 2.2 Linewidth as a function of size, $R_{\rm S}$, for simulated (black stars) and observed (grey symbols) molecular clouds. The observational data was obtained from Table 1 of Heyer et al. (2009) for clouds with areas determined by Solomon et al. (1987), A_1 (open diamonds), and by the half-max isophote of peak column density, A_2 (open triangles).

lie on the Larson size-linewidth relation (black dashed line) and are shown to have comparable velocity dispersions to observed clouds, for sizes ranging from 3 – 20 pc. Due to the nature of our cloud selection, our cloud sizes are limited to a finite range. Our largest simulation is approximately 60 pc across, therefore our selected cloud regions are necessarily smaller. There is also a lower limit to our cloud sizes as regions less than 3 pc across are deemed too small to be considered clouds for our sample (see Section 2.3).

We draw the reader's attention to the presence of large scatter about the relation in both the observational data and simulated data. Some of this scatter can be attributed to variable cloud surface densities. Using the size definition of Equation 2.4, we determined the size-linewidth coefficient, $v_{\rm o} = \sigma_{\rm 1D}/{R_{\rm S}}^{0.5}$, for each of our clouds. In Fig. 2.3, we plot $v_{\rm o}$ as a function of the cloud mass surface density, $\Sigma = M/\pi {R_{\rm S}}^2$. We see that the surface density varies by approximately two orders of magnitude and that the scatter in this relation is greatly reduced as compared to that seen in the size-linewidth relation (Fig. 2.2). Our data show an even stronger correlation between the size-linewidth coefficient and the surface density than that seen by Heyer et al. (2009) with a Pearson correlation coefficient of 0.73. Within the range of mass surface densities probed by Heyer et al. (2009), a fit to the data has the following functional form

$$v_{\rm o} \propto \Sigma^{0.49\pm0.04}, \tag{2.5}$$

as expected for clouds which are gravitationally bound and in virial equilibrium. However, recall that this sample is populated by both bound and unbound clouds, simulated including only turbulence and gravity. Our result indicates that the $v_{\rm o}$-Σ relation does not require mechanisms such as magnetic fields, variable external pressure, or stellar feedback and that the accompanying scatter may be due to the boundedness (or unboundedness) of the molecular clouds. This interpretation of the scatter will be explored further in Section 2.4.3.

While Heyer et al. (2009) measured their properties over the entirety of the cloud within an area pre-defined by Solomon et al. (1987), an alternate method of determining cloud area is by counting the number of pixels in an extinction

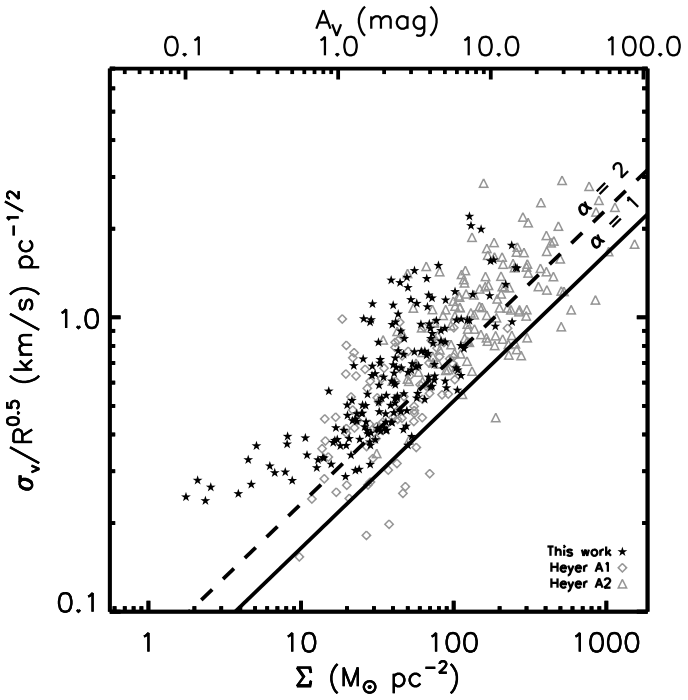

Figure 2.3 Size-linewidth coefficient, $v_{\rm o}$, as a function of cloud mass surface density, Σ, for the molecular cloud sample using the Solomon et al. (1987) definition of cloud size, $R_{\rm S}$ (black stars), as compared to the observational data of Heyer et al. (2009) (grey symbols). The dashed line represents the boundary below which clouds are considered gravitationally bound ($\alpha = 2$) and the solid line represents the boundary at which clouds are virialised ($\alpha = 1$). The simulated clouds follow the observed $v_{\rm o}$-Σ trend of Heyer et al. (2009) with a Pearson correlation coefficient of 0.73.

map which are above a given threshold and multiplying by the surface area of each pixel (e.g. Lombardi et al., 2010). We calculated the area of our own maps in this way above the minimum column density threshold (0.5×10^{21} cm^{-2}). A primary concern for extinction-based data is the high levels of background noise in the maps. However, since we do not have any noise in our simulations, we can analyse our synthetic observations as extinction maps without concern of contamination from the background. The mass surface density is therefore equal to the mass above the threshold, M, divided by the surface area above the threshold, A, and the effective radius, $R_{\rm L}$, is

$$R_{\rm L} = \sqrt{\frac{A}{\pi}}. \tag{2.6}$$

Using this definition of cloud size, we re-derived our cloud properties. Fig. 2.4 shows $v_{\rm o} = \sigma_{\rm 1D}/{R_{\rm L}}^{0.5}$, as a function of $\Sigma = M/\pi {R_{\rm L}}^2$. A fit to the data plotted in Fig. 2.4 shows that the size-linewidth coefficient, $v_{\rm o}$, is again proportional to $\Sigma^{1/2}$ as expected from Equation 2.2. We also calculated the mean surface density to be $\bar{\Sigma} = 38 \pm 4$ M$_\odot$ pc^{-2}, which is consistent with the median surface density of 42 M$_\odot$ pc^{-2} reported by Heyer et al. (2009).

Lombardi et al. (2010) found from their observations that cloud column densities are *constant* above a given threshold and that their value is dependent on the threshold. We tested this result for our clouds by recalculating the cloud properties for three higher thresholds ($A_{\rm v} \geq 1$). We find that if a cloud is probed to very low extinctions, the $v_{\rm o}$-Σ relation can be recovered; otherwise, the surface density will appear to be roughly constant since the range of surface densities becomes limited (e.g. Kauffmann et al., 2010a; Lombardi et al., 2010). Since the lower limit for detection in current observations is $A_{\rm v} \sim 0.5$ (Kainulainen et al., 2009; Beaumont et al., 2012), extinction-based data will

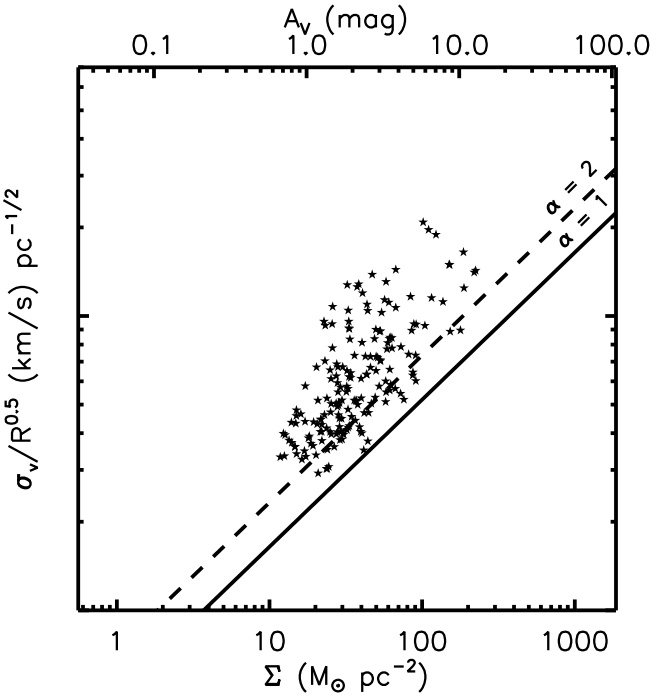

Figure 2.4 Size-linewidth coefficient, $v_{\rm o}$, as a function of cloud mass surface density, Σ, for the molecular cloud sample using the Lombardi et al. (2010) definition of cloud size, $R_{\rm L}$. The boundaries below which clouds are considered gravitationally bound (dashed line, $\alpha = 2$) and virialised (solid line, $\alpha = 1$) are also shown.

naturally result in a constant column density since the threshold is necessarily too high (typically $A_{\rm v} > 1$).

2.4.2 Determining an appropriate size estimator

We have explored two methods for defining cloud size which give similar results. However, which is the best way to characterise a cloud's size? A definition of size that provides an accurate estimate of the gravitational potential energy is particularly useful in order to estimate the virial parameter.

Using three-dimensional information from the simulations we can define a cloud's size using the gravitational potential (Smith et al., 2009; Gong & Ostriker, 2011). We can determine the gravitational potential energy, U, for each cloud in our sample as follows,

$$U = \sum_i \frac{1}{2} m_i \phi_i, \tag{2.7}$$

where m_i is the mass and ϕ_i is the gravitational potential of each particle in the cloud. As mentioned previously, we only included particles contained in pixels above a minimum column density threshold of $0.5{\times}10^{21}$ cm^{-2} in our determination of cloud properties. We have also included sink particles in our calculation of the gravitational potential energy and total mass of the cloud. Using the gravitational potential energy, we then derive a radius, $R_{\rm pot}$:

$$R_{\rm pot} = \frac{3}{5} \frac{GM^2}{|U|}, \tag{2.8}$$

where M is the total mass of the cloud and stars. We find that our estimate of the radius, $R_{\rm pot}$, is not affected by the inclusion of sink particles. The factor of 3/5 assumes that the clouds can be represented as homogeneous spheres, which is a common assumption when deriving properties of molecular clouds. This coefficient varies by less than 25 percent for clouds that are more accurately represented as 1:2 prolate or oblate homogeneous ellipsoids and we conclude that a sphere is a fair approximation for the global shape of a molecular cloud.

If we compare $R_{\rm pot}$ to the estimates for cloud radius derived from the two methods that we have previously explored, we can determine the best observational estimate of cloud size for the specified purpose of finding the boundedness of a cloud. Fig. 2.5 shows the two observational estimates of radius plotted as a function of $R_{\rm pot}$. Both observed radii are quite representative of

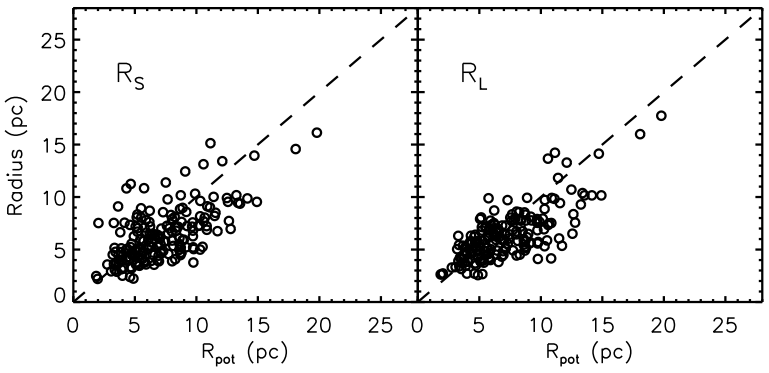

Figure 2.5 Observed radius as a function of $R_{\rm pot}$. The dashed one-to-one line is also shown. The observed radii are the effective radius from Solomon et al. (1987) (left) and the effective radius from Lombardi et al. (2010) (right).

the full radius of the cloud as determined by the gravitational potential energy. The radii as determined by the method of Lombardi et al. (2010) are slightly more correlated with $R_{\rm pot}$ with a Pearson coefficient of 0.75 compared to a Pearson coefficient of 0.65 for the radii as determined by the Solomon et al. (1987) method. The principal variation from cloud to cloud is its shape which gives rise to the scatter seen in Fig. 2.5. Clouds which are highly non-spherical will result in an overestimation of cloud size by the method of Solomon et al. (1987). These results indicate that the method for determining the cloud radius outlined in Lombardi et al. (2010) is a more useful means of characterising the size of a cloud with respect to its virial state.

2.4.3 Do unbound clouds match observations?

In the previous section, we determined that the most appropriate measure of a cloud's size can be made using the method of Lombardi et al. (2010). From the masses, linewidths, and sizes as defined by Lombardi et al. (2010) for the molecular clouds in our sample, we determine the virial parameter of each cloud. We note that a large fraction of the clouds are strictly unbound ($\alpha > 2$).

In Section 2.4.1, we interpreted the scatter in Figs 2.3 and 2.4 as being due to a spread in the virial parameter. By definition, the size-linewidth coefficient not only depends on the mass surface density, but it is also dependent on the virial parameter, α:

$$v_{\rm o} = (\pi G \alpha \Sigma / 5)^{1/2}. \tag{2.9}$$

However, the virial parameter is commonly assumed to be a constant rather than a property capable of variation. Heyer et al. (2009) assumed that $\alpha = 1$ and thus disregarded the virial parameter from their arguments concerning the scatter in the relation between the size-linewidth coefficient and the surface density. If we consider the idea that clouds may not necessarily be gravitationally bound or virialised ($\alpha \neq 1$, see Section 2.1), the scatter can be explained by the boundedness (or unboundedness) of the molecular cloud.

In order to determine whether the observed virial parameter defined by Equation 2.1 is actually reflective of the true virial state of the cloud, we calculated the physical virial parameter given by

$$\alpha_{\rm 3D} = 2K/U, \tag{2.10}$$

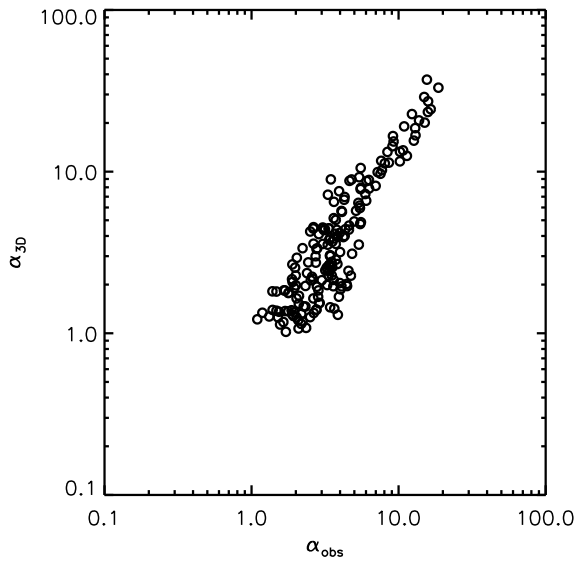

Figure 2.6 True physical virial parameter, $\alpha_{3D} = 2K/U$, as a function of the observed virial parameter, $\alpha_{obs} = 5\sigma^2 R/GM$.

where U is the gravitational potential energy determined by Equation 2.7 and K is the kinetic energy determined from the mass of the cloud and stars, M_{tot}, and one-dimensional velocity dispersion, σ_{1D}, such that

$$K = \frac{3}{2} M_{tot} \sigma_{1D}^2. \tag{2.11}$$

Fig. 2.6 shows the tight correlation between the observed and physical virial parameters, indicating that many of the molecular clouds in our sample ($> 69\%$) are truly unbound with $\alpha_{3D} > 2$. Therefore, a measure of the virial parameter using an appropriate size estimator is representative of the true virial state of the molecular cloud, which characterises the amount of scatter in the v_o-Σ relation.

In previous sections, we found that our clouds, which range from bound to unbound as defined by their true virial state, match the observational trends.

As shown above, we also find that observational estimates of cloud virial parameters should be close to the true values. It is thus reasonable to take the observations at face value and assume that a substantial fraction of real molecular clouds are unbound.

2.5 Conclusions & Discussion

We studied the properties of a sample of molecular clouds with masses ranging from $\sim$ 300 – 10 000 $M_\odot$, which were formed within larger volumes and simulated with only turbulence and gravity. This sample follows the observed trend of the size-linewidth coefficient, $v_o = \sigma_v / R^{1/2}$, with the surface density, Σ, from Heyer et al. (2009). We also argued that the virial state, and consequently the boundedness, of a molecular cloud is the source of the scatter which accompanies the trend. We have shown that the observed properties can be understood if molecular clouds are a population of turbulent, transient, and often unbound structures. This interpretation is consistent with the data of both Heyer et al. (2009) and Larson (1981). These findings support the idea that clouds need not be maintained in dynamical equilibrium ($\alpha = 1$). Recent work by Kritsuk et al. (2013), using periodic mesh simulations, reached similar conclusions. This implies that additional support from magnetic fields, variable external pressure, or stellar feedback may be less important than is commonly assumed.

Assuming virialized clouds is likely to provide erroneous mass estimates. However, if we cannot assume virialization, this raises the question of how to estimate α for a molecular cloud based on observable quantities. We noted in Section 2.4.1 that the surface density is relatively constant above high thresh-

olds, consistent with the results of Lombardi et al. (2010) and Kauffmann et al. (2010a). Therefore, provided that we can measure the size and linewidth of a molecular cloud, we can solve for the virial parameter, α, and its mass, assuming a functional dependence of the column density on the chosen threshold (see also Ballesteros-Paredes et al., 2012). We find that the estimate of cloud size as determined from extinction maps (e.g. Lombardi et al., 2010) provides an accurate way to determine the cloud's gravitational potential energy and, subsequently, its virial parameter.

We find that all clouds in our sample ultimately form collapsing cores, regardless of whether the cloud is bound, consistent with the results of Clark et al. (2005). Localised regions of compression due to turbulence within unbound clouds lead to isolated regions of star formation as the clouds disperse and their column density fades beneath the lower limit for detection. We conclude that molecular clouds do not have to be bound to form stars or to have observed properties like those of nearby low-mass clouds. If molecular clouds are unbound, this allows for relatively low star formation rates for individual clouds, matching those seen in observations. These low star formation rates are naturally produced for unbound clouds as they are not directly tied to their free-fall times. We will explore the evolution of cloud properties, including the star formation rate, in future work. Since our simulations are roughly scale-free, we expect our results to apply to clouds of higher masses as well. A substantial role for unbound clouds could help resolve the long standing issue of low galactic star formation rates despite the abundance of molecular gas.

2.6 Acknowledgments

We would like to thank SHARCNET (Shared Hierarchical Academic Research Computing Network) and Compute/Calcul Canada, which provided dedicated resources to run these simulations. This work was supported by NSERC. J.W. acknowledges support from the Ontario Early Researcher Award (ERA). The authors would like to thank the anonymous referee for useful comments that have improved this work.

Bibliography

Arce, H., Borkin, M. A., Goodman, A. A., Pineda, J. E., & Halle, M. W. 2010, ApJ, 715, 1170

Arzoumanian, D., André, P., Didelon, P., et al. 2011, A&A, 529, 6

Ballesteros-Paredes, J., D'Alessio, P., & Hartmann, L. 2012, MNRAS, 427, 2562

Ballesteros-Paredes, J., Hartmann, L. W., Vázquez-Semadeni, E., Heitsch, F., & Zamora-Avilés, M. A. 2011, MNRAS, 411, 65

Bate, M. R. & Bonnell, I. A. 2005, MNRAS, 356, 1201

Beaumont, C. N., Goodman, A. A., Alves, J. F., et al. 2012, MNRAS, 423, 2579

Bergin, E. A. & Tafalla, M. 2007, ARA&A, 45, 339

Bertoldi F. & McKee C. F. 1992, ApJ, 395, 140

Bohlin, R. C., Savage, B. D., & Drake, J. F. 1978, ApJ, 224, 132

Bonnell, I. A., Smith, R. J., Clark, P. C., & Bate, M. R. 2011, MNRAS, 410, 2339

Clark, P. C., Bonnell, I. A., Zinnecker, H., & Bate, M. R. 2005, MNRAS, 359, 809

Clark, P. C., Bonnell, I. A., & Klessen, R. S. 2008, MNRAS, 386, 3

Dobbs, C. L., Burkert, A., & Pringle, J. E. 2011, MNRAS, 413, 2935

Elmegreen, B. 1989, ApJ, 338, 178

Federrath, C., Banerjee, R., Clark, P. C., & Klessen, R. S. 2010, ApJ, 713, 269

Field, G. B., Blackman, E. G., & Keto, E. R. 2011, MNRAS, 416, 710

Gong, H. & Ostriker, E. C. 2011, ApJ, 729, 120

Goodman, A. A., Pineda, J. E., & Schnee, S. L. 2009, ApJ, 692, 91

Heyer, M. H., Carpenter, J. M., & Snell, R. L. 2001, ApJ, 551, 852

Heyer, M., Krawczyk, C., Duval, J., & Jackson, J. M. 2009, ApJ, 699, 1092

Kainulainen, J., Lada, C. J., Rathborne, J. M., & Alves, J. F. 2009, A&A, 497, 399

Kainulainen, J., Federrath, C., & Henning, T. 2013, A&A, 553, 8

Kauffmann, J., Pillai, T., Shetty, R., Myers, P. C., & Goodman, A. A. 2010a, ApJ, 712, 1137

Kauffmann, J., Pillai, T., Shetty, R., Myers, P. C., & Goodman, A. A. 2010b, ApJ, 716, 433

Kritsuk, A. G., Lee, C. T. & Norman, M. L. 2013, MNRAS, 436, 3247

Lada, C. J., Lombardi, M., & Alves, J. F. 2009, ApJ, 703, 52

Larson, R. B. 1981, MNRAS, 194, 809

Lombardi, M., Alves, J., & Lada, C. J. 2010, A&A, 519, 7

Men'shchikov, A., André, P., Didelon, P., et al. 2010, A&A, 518, 103

Monaghan, J. J. and Lattanzio, J. C. 1985, A&A, 149, 135

Mouschovias, T. Ch. 1987, in Physical Processes in Interstellar Clouds, ed. G. E. Morfill & M. Scholer (Dordrecht: Reidel), 453

Petitclerc, N. 2009, PhD Thesis, McMaster University

Pineda, J. L., Goldsmith, P. F., Chapman, N., et al. 2010, ApJ, 721, 686

Smith, R. J., Clark, P. C., & Bonnell, I. A. 2009, MNRAS, 396, 830

Solomon, P. M., Rivolo, A. R., Barrett, J. & Yahil, A. 1987, ApJ, 319, 730

Wadsley, J. W., Stadel, J., & Quinn, T. 2004, New Astronomy, 9, 137

Ward, R. L. "Connecting the Dots: Comparing SPH Simulations and Synthetic Observations of Star-forming Clumps in Molecular Clouds" (2011). M.Sc. Thesis, McMaster University, Open Access Dissertations and Theses. Paper 6283.

Ward, R. L., Wadsley, J., Sills, A., & Petitclerc, N. 2012, ApJ, 756, 119

Wilson, C. D. & Scoville, N. 1990, ApJ, 363, 435

Wong, T., Hughes, A., & Ott, J. et al. 2011, ApJS, 197, 16

Chapter 3

Evolving Molecular Cloud Structure and the Column Density Probability Distribution Function

Reprinted from Rachel L. Ward, James Wadsley, and Alison Sills, 2014, Monthly Notices of the Royal Astronomical Society*, Volume 445, Issue 2, pp. 1575–1583, DOI: 10.1093/mnras/stu1868. Published by Oxford University Press on behalf of the Royal Astronomical Society.*

Abstract

The structure of molecular clouds can be characterized with the probability distribution function (PDF) of the mass surface density. In particular, the properties of the distribution can reveal the nature of the turbulence and star formation present inside the molecular cloud. In this paper, we explore how these structural characteristics evolve with time and also how they relate to various cloud properties as measured from a sample of synthetic column density maps of molecular clouds. We find that, as a cloud evolves, the peak of its column density PDF will shift to surface densities below the observational threshold for detection, resulting in an underlying lognormal distribution which has been effectively lost at late times. Our results explain why certain observations of actively star-forming, dynamically older clouds, such as the Orion molecular cloud, do not appear to have any evidence of a lognormal distribution in their column density PDFs. We also study the evolution of the slope and deviation point of the power-law tails for our sample of simulated clouds and show that both properties trend towards constant values, thus linking the column density structure of the molecular cloud to the surface density threshold for star formation.

3.1 Introduction

Giant molecular clouds (GMCs) are large regions of gas and dust, which undergo local gravitational collapse to form dense star-forming cores. The morphology and structure of GMCs are significantly affected by the presence of turbulence which is highly supersonic on large-scales and leads to the formation of density enhancements such as filaments, clumps, and cores within which star formation occurs.

The probability distribution function (PDF) of the mass density is one representation of the role of supersonic turbulence on the structure of molecular clouds. Many numerical studies (e.g. Vázquez-Semadeni, 1994; Nordlund & Padoan, 1999; Ostriker et al., 2001; Padoan & Nordlund, 2002; Krumholz & McKee, 2005; Hennebelle & Chabrier, 2008) have shown that a lognormal shape is expected for the density PDF of an isothermal, supersonic turbulent gas.

Recent observations by Kainulainen et al. (2009) showed that column density PDFs for molecular clouds also exhibit a lognormal distribution. However, they observed this distribution only in quiescent clouds which are not actively undergoing star formation. The column density PDFs for star-forming molecular clouds, such as the Taurus Molecular Cloud, have an underlying lognormal shape with the addition of a power-law tail at high column densities. This distribution is reminiscent of the stellar initial mass function (IMF) whose form is often approximated either by a lognormal (Chabrier, 2003) or by a power-law (Salpeter, 1955; Kroupa, 2001) at the high-mass end of the spectrum. These results suggest that characterising the shape of the density and column density

PDF of molecular clouds is crucial for understanding the origin of the stellar IMF.

Several numerical studies (Tassis et al., 2010; Ballesteros-Paredes et al., 2011; Kritsuk et al., 2011) have subsequently confirmed the presence of a power-law tail in the density and column density PDFs from three-dimensional simulations of molecular clouds collapsing to form stars. These authors argue that the tail develops over time and its strength grows as more stars are formed and as gravity becomes dominant over turbulence.

Kainulainen et al. (2011) explored the nature of the transition from a log-normal shape at low column densities to a power-law shape at higher column densities for actively star-forming clouds. The authors showed that the changing shape of the PDF can be interpreted as the transition from a diffuse cloud dominated by turbulence to a clumpy gravitationally-dominated structure. Kainulainen et al. (2011) showed that the 'structural transition' of the PDF offers a physical explanation for the star formation threshold and for the correlation between the star formation rate and the mass of dense gas above the threshold in molecular clouds (Lada et al., 2010). Throughout this paper, we will refer to the threshold at which the structural transition occurs as $\Sigma_{\rm tail}$ where all gas above this threshold is considered dense enough to form stars.

There are several properties of the distribution which characterise the shape of the column density PDF for molecular clouds. In this paper, we explore how these structural characteristics evolve with time and also how they relate to various cloud properties as measured from a sample of synthetic column density maps of bound and unbound molecular clouds. Column density PDFs derived from molecular cloud observations can be ordered into an assumed

sequence to demonstrate the evolutionary process from lognormal shape to the development of a power-law tail. Simulators have shown this to be the case; however, the evolution of column density PDFs of simulated clouds in an observational context has not yet been considered. Observational limits and thresholds naturally interfere with estimates of cloud properties. In this paper, we show that thresholds can significantly affect the way we interpret molecular cloud structure and evolution, particularly for older, actively star-forming clouds like the Orion molecular cloud.

In Section 3.2, we review the details of our simulations, the methods used to produce our synthetic column density maps, and the criteria for cloud selection first outlined in Ward et al. (2014). We describe our method of tracking clouds through time and present our findings on the evolution of their structural properties in Section 3.3. Lastly, in Section 3.4, we summarize our results and discuss the implications of our conclusions.

3.2 Methods

We use simulations of molecular clouds to study the evolution of their structure and its effect on star formation. Simulations allow us to explore the three-dimensional properties of the cloud in order to better understand the two-dimensional properties which are observed. We created column density projections of our simulations to compare more directly to observations. The dynamic properties of our synthetic clouds were the subject of a previous study by Ward et al. (2014) and full details of the simulations, column density maps, and the cloud selection process are provided in that paper. What follows is a brief overview highlighting the key details of our method.

Table 3.1 Initial Conditions for the Simulations

Id	Radius (pc)	σ_{3D} (km s^{-1})	$n_{initial}$ (cm^{-3})	t_{ff} (Myr)	$\alpha_{initial}$
9	30	2.93	7.69	22.4	2
10	21.2	3.49	21.8	13.3	2
11	15	4.15	61.5	7.9	2
12	10.6	4.93	174	4.7	2
13	30	2.07	7.69	22.4	1
14	21.2	2.47	21.8	13.3	1
15	15	2.93	61.5	7.9	1
16	10.6	3.49	174	4.7	1

Note. — Reproduction of table 1 from Ward et al. (2014)

Our synthetic clouds were selected from initially bound 50 000 $M_\odot$ regions of the ISM, simulated using the smoothed particle hydrodynamics code Gasoline (Wadsley et al., 2004). Throughout this paper we only consider the cases where the initial global virial parameter of the volumes is less than or equal to 2 (or gravitationally bound) to avoid rapid dispersal due to high turbulent motions. The initial conditions for these cases cover a range of initial densities and Mach numbers listed in Table 1 of Ward et al. (2014) for volumes labelled by IDs 9 - 16. This table with the relevant cases has been reproduced for this work (Table 1). Our particle mass is 8.85 $\times$ 10^{-3} $M_\odot$ with a mass resolution limit for fragmentation of 0.6 $M_\odot$, resulting in simulations which are highly resolved and include only gravity and decaying turbulence with large-scale modes in non-periodic boxes. We use the Bate & Bonnell (2005) equation of state, whose opacity limit for fragmentation is greater than our maximum gas density, resulting in simulations which are entirely optically thin and isothermal at 10 K. As a result, our column density projections are equivalent to

synthetic observations derived from radiative transfer calculations in the limit of optically thin gas. Detailed descriptions of the methods used to produce our synthetic column density maps can be found in Ward et al. (2012, 2014). Approximately 60 clouds at various stages of their evolution were selected from the column density maps of each turbulent region using surface density contours to identify the peak emission. The selection process ensures that the clouds in our sample have column densities which exceed the lower limit for detection in dust extinction measurements ($A_V \sim 0.5$; Kainulainen et al., 2009; Beaumont et al., 2012). This limit also approximates the threshold at which atomic hydrogen begins to self-shield against UV radiation ($\sim 10^{20-21}$ cm^{-2}) leading to the formation of molecular hydrogen. These synthetic clouds have sizes and surface densities which are analogous to observed molecular clouds, allowing for a more direct comparison to observations. The spatial resolution of our column density maps is 6000 AU px^{-1}, which corresponds to an angular resolution of ~ 45 arcsec for a cloud at a distance of 140 pc, such as the Taurus molecular cloud (Nutter et al., 2008).

Although the simulation volumes are bound overall with global virial parameters ≤ 2, the clouds within the volume have local virial parameters ranging from 0.5 to 6.5 due to localised regions of collapse and turbulence. Of the 58 clouds in our sample, over 30% are gravitationally bound with local virial parameters ≤ 2. This allows us to explore the structural evolution of both bound and unbound clouds, since the local virial parameters of the clouds remain steady and evolve minimally for the duration of the simulations.

We used sink particles to represent the high density regions of the simulations (inserted at densities greater than 10^6 cm^{-3}) based on the formation

criteria of Federrath et al. (2010). Each sink corresponds to a star-forming core or a cluster-forming core with a radius of 500 AU. We find that all of our clouds eventually form stars regardless of whether or not they are bound overall. Since our simulations do not model radiative feedback, we do not include clouds in our study which have converted more than 35% of their mass to stars.

3.3 Results

In order to compare directly to observations, we only included the pixels from our maps with surface densities greater than ~ 10 $M_\odot$ pc^{-2}. This minimum surface density corresponds to the threshold for detection in extinction maps – $A_V \sim 0.5$ (Kainulainen et al., 2009) where the conversion factor is $\Sigma/A_V = 20$ $M_\odot$ pc^{-2} mag^{-1} (Bohlin et al., 1978; Lombardi et al., 2010; Kainulainen et al., 2011; Lombardi et al., 2014). We also removed the sink particles from our column density maps, which is common practice for the case of embedded stars in studies of molecular clouds (in CO and extinction-based data) due to their tendency to bias measurements (Goodman et al., 2009; Kainulainen et al., 2009; Kainulainen, Federrath, & Henning, 2013).

To demonstrate that we can sensibly track the evolution of our clouds, a bound 10^4 $M_\odot$ cloud selected at $t = 4.0$ Myr is shown in Figs 3.1 and 3.2 to evolve in two possible ways. For the true evolution (shown by the solid arrow), gas particles present in a column density map at $t = 4.0$ Myr are marked using their particle ids from the simulation, extracted from the simulation volume, and evolved forward in time. This allows us to study the dynamics of the particles, as they are isolated from the surrounding medium. For the

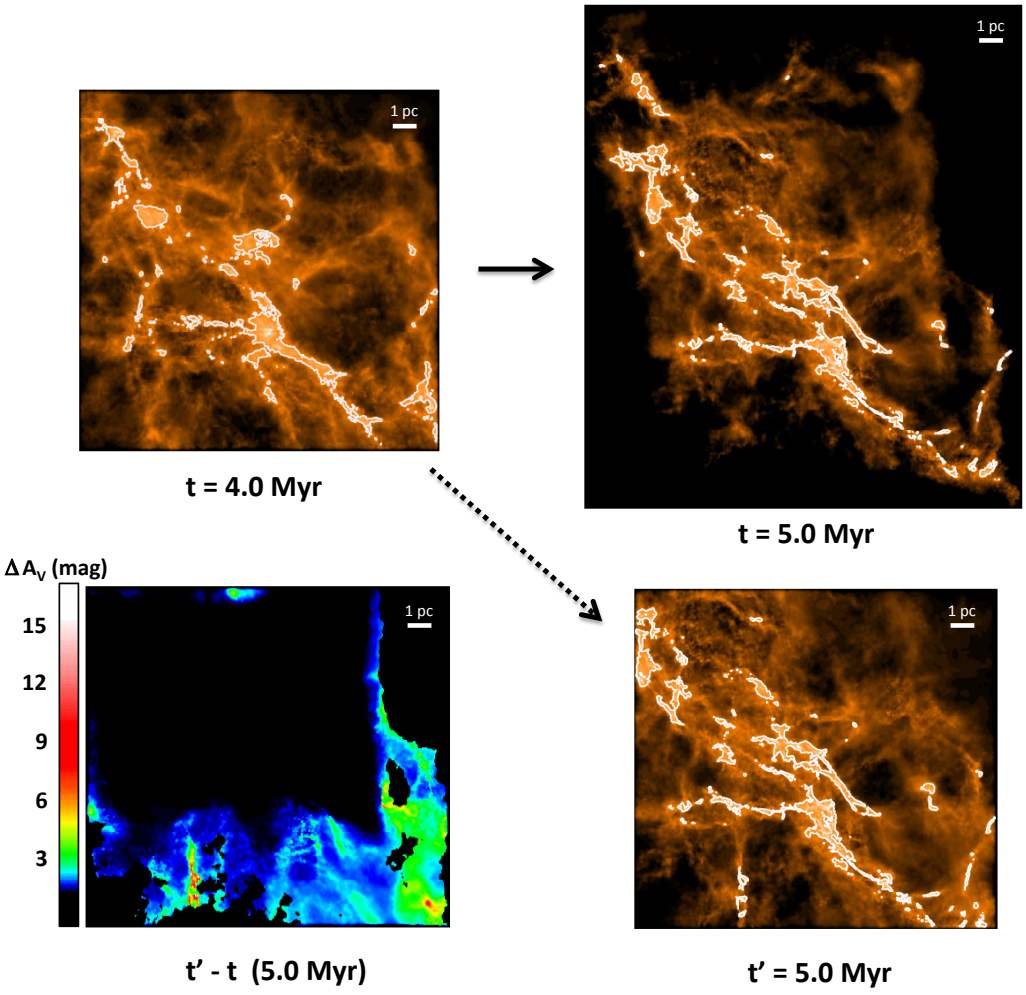

Figure 3.1 Synthetic column density maps for the evolution of a single cloud. The solid arrow shows the actual evolution of the particles from t=4.0 to t=5.0 Myr and the dotted arrow shows the perceived evolution of the cloud taken from independent snapshots at t=4.0 Myr and t'=5.0 Myr using an observationally-motivated selection criteria. The contours outline regions with visual extinctions greater than 8 mag. The $t' - t$ difference map at 5.0 Myr is shown in the bottom left corner.

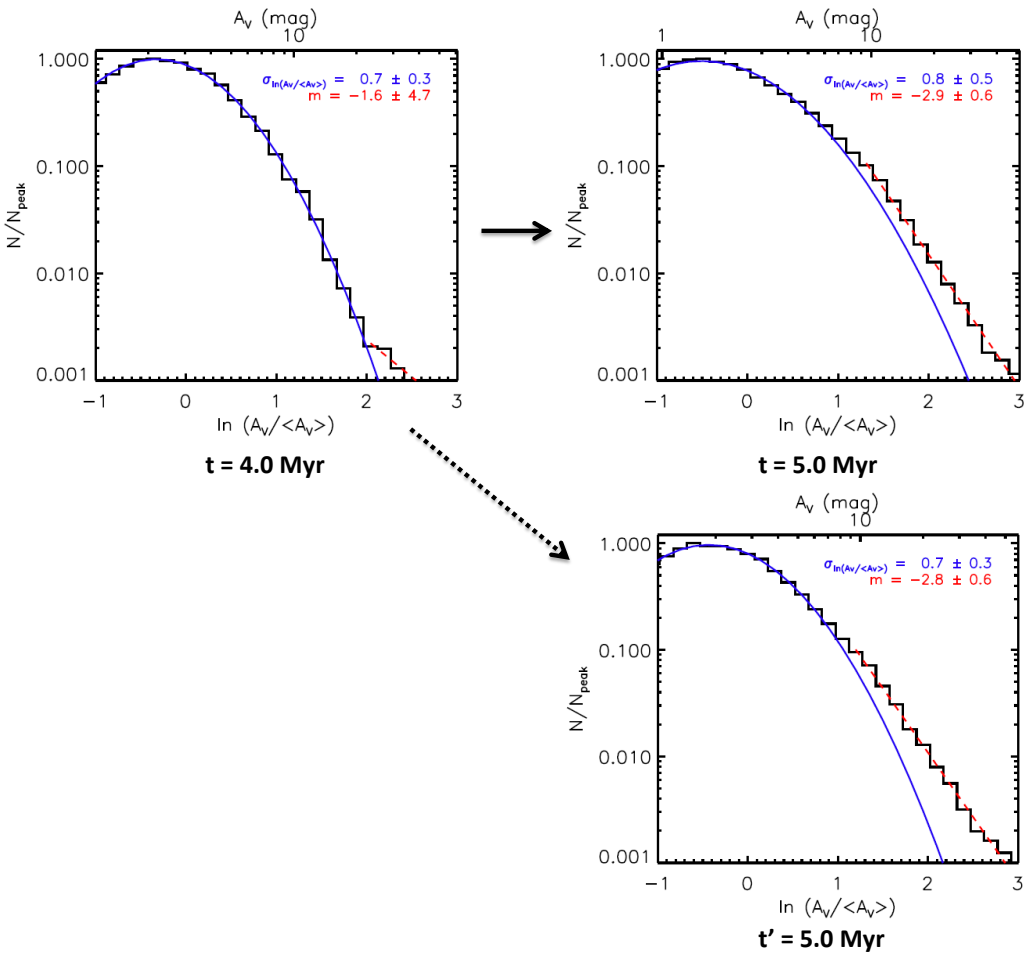

Figure 3.2 Column density PDFs for the evolution of a single cloud. The column density PDFs are normalized by the peak of the distribution and are plotted as a function of the mean-normalized extinction, $\ln(A_V/\langle A_V \rangle)$. The solid line shows the lognormal fit to the distribution and the dashed line shows the power-law fit to the tail of the distribution.

perceived evolution (shown by the dotted arrow), we take two independently selected clouds: one in the 4.0 Myr snapshot and one in the 5.0 Myr snapshot. If two clouds selected in this way have x-y positions in the map which are close, we claim that the older cloud is the evolved version of the younger cloud. This method based on appearance is analogous to what observers do to better understand cloud evolution. We note from Fig. 3.1 that the two outcomes are quite alike in appearance; however, they are also similar in their bulk properties, such as their maximum surface densities and in the amount of mass in dense gas. We also find that both methods of tracking the evolution of the cloud result in column density PDFs that are in agreement within uncertainties as seen in Fig. 3.2. Therefore, our method of tracking cloud evolution is robust as the effects of the surrounding environment are minor and do not significantly influence the structural evolution of the cloud during the timescales of interest (on the order of a free-fall time, $t_{\rm ff}$). We will explore the effect of environment on longer timescales in future work for clouds formed in a galactic disc.

We follow the evolution of each of our ~ 60 clouds forward in time, producing a column density map after each 1 Myr time interval. For each column density map, we produced a corresponding column density PDF plotted over a range chosen to match the observations of Kainulainen et al. (2009). To study the evolution of the molecular cloud structure in detail, we focus on the defining characteristics of the column density PDF. The shape of the PDF is characterised by four key structural properties: its width (σ), peak location (Σ_{peak}), the slope of the power-law (m), and the deviation point (Σ_{tail}). These properties are identified in the diagram shown in Fig. 3.3.

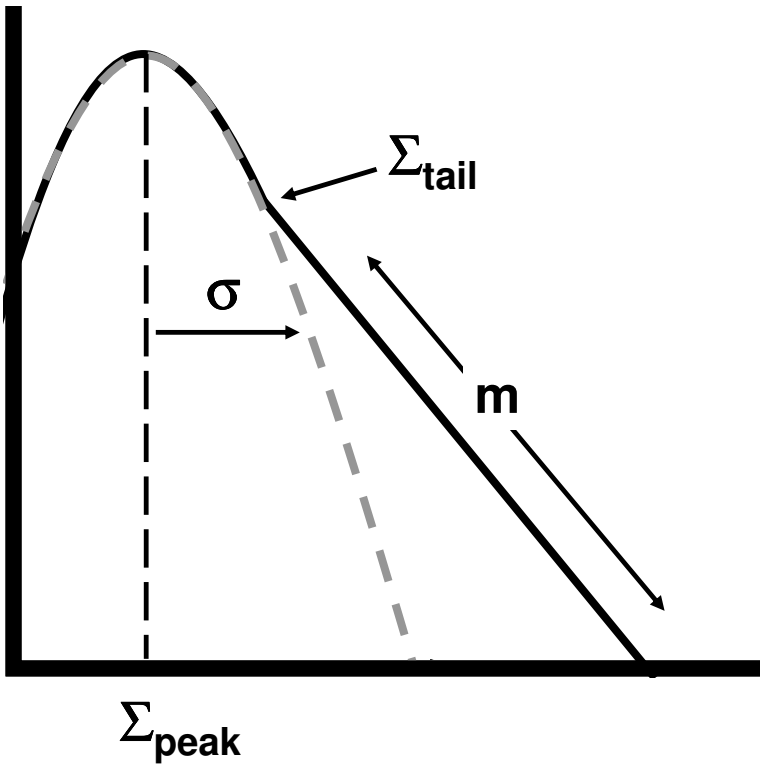

Figure 3.3 Schematic diagram of the mass surface density probability distribution function (PDF). The structural properties of interest are the peak, $\Sigma_{\rm peak}$, and width of the distribution, σ, the slope of the power-law tail, m, and the surface density at which the power-law tail first forms, $\Sigma_{\rm tail}$.

The peak and width of the distribution are determined by fitting the log-normal function

$$p(\zeta) = \frac{1}{\sqrt{2\pi\sigma_\zeta^2}} \exp\left[-\frac{(\zeta-\mu)^2}{2\sigma_\zeta^2}\right] \tag{3.1}$$

to the low extinction range of the PDF between $\zeta = \ln(A_V/\langle A_V\rangle) = [-1,1]$ (Kainulainen et al., 2009; Schneider et al., 2014) where μ and σ_ζ are the mean logarithmic column density and dispersion respectively. The deviation point, $\Sigma_{\rm tail}$, is defined as the value of ζ where the data deviates from the lognormal fit by a factor of 1.25 (dashed lines in Fig. 3.2). This definition of the deviation point coincides with the values which would be identified by eye. The power-law slopes are fit between the deviation point and the surface density at which $N/N_{\rm peak} = 0.001$, below which the signal would be too low to be detected observationally.

At early times ($t \sim 0.1\ t_{\rm ff}$), we find that the clouds appear diffuse and turbulent, exhibiting a lognormal distribution. At later times after the sinks have begun to form ($t \sim 0.6\ t_{\rm ff}$), the distributions have developed a power-law tail along with an underlying lognormal shape, which is significantly wider with a lower peak column density (Fig. 3.4). To illustrate the characteristics of the structural transition and the times at which these transitions occur, we plotted the evolution of the four column density PDF properties for our clouds in Fig. 3.5.

Clouds which could not be fit by a lognormal due to evolution of the peak to extinction values below the minimum threshold were excluded from Figs 3.5(a) and 3.5(b) and are not considered in subsequent sections. Since it was still possible to fit power-law slopes to these clouds, they are included in Figs 3.5(c) and 3.5(d) and are considered in later discussions.

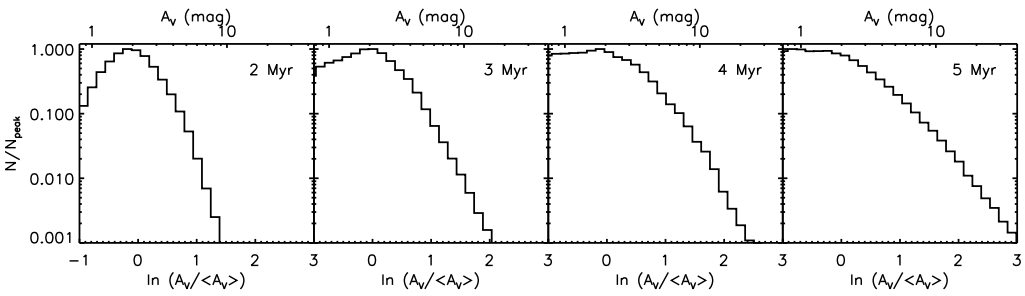

Figure 3.4 Evolution of the column density PDF for a typical molecular cloud. Each PDF is normalized by the peak of its distribution and plotted as a function of the mean-normalized extinction, $\ln(A_V/\langle A_V \rangle)$.

In Fig. 3.5(a), we see that the peak of the distribution decreases as a function of time. We see this trend for both bound and unbound clouds. However, the peak of the distribution cannot evolve to surface densities any lower than the imposed threshold. Therefore, there may be a significant amount of mass in clouds which exists below the threshold for detection. This indicates that observational limitations can greatly impact the number of molecular clouds identified at late stages of their evolution.

Lombardi et al. (2014) find no evidence of lognormality in their PDFs of the Orion star-forming region using data from *Herschel* and *Planck*. The authors suggest that the lognormal could be confined to low column densities ($<$ $A_V \sim 1$ mag) below what they are able to detect and argue that the power-law regime dominates and characterises the majority of cloud structure. We show that this is indeed the case for 'old' clouds – clouds which have been actively star-forming for several Myrs, like Orion. Although stars are consuming gas, the amount of dense gas ($n > 10^4$ cm^{-3}) available for star formation tends to remain relatively constant over time due to accretion and dispersal. These

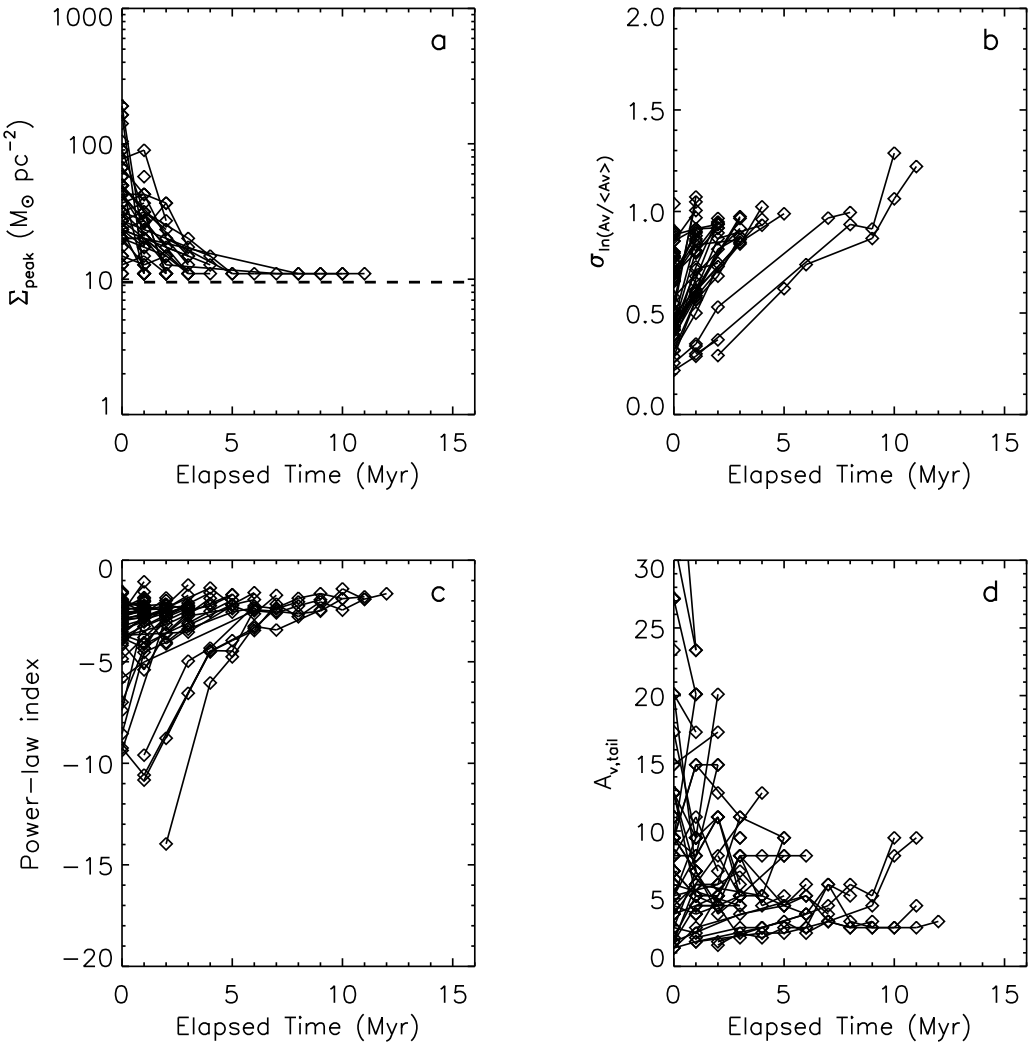

Figure 3.5 Evolution of the structural properties of molecular cloud surface density PDFs: a) Peak surface density ($\Sigma_{\rm peak}$), b) width ($\sigma_{\ln(A_V/\langle A_V\rangle)}$), c) power-law slope ($m$), and d) tail deviation point ($A_{V,\rm tail}$) as a function of time. The solid lines show the evolutionary tracks for each cloud. The dashed line shows the minimum surface density corresponding to the threshold for detection in observations.

clouds have begun dispersing the low column density gas and are rapidly converting high column density gas into stars, the net result of which is a lowering of the overall peak column density of the lognormal distribution. The younger (or less evolved) a cloud is, the more likely a lognormal distribution will be observed in its PDF. Alternatively, older star-forming regions will be dominated solely by a power-law as their distributions have evolved to peak below the current limits of detection by observations. Fig. 3.6 shows the PDF for a cloud in our sample which would be identified as having a power-law across the entire range of column densities within the observed limits ($A_V > 1$ mag); however, we can see that the lognormal is still present, but now shifted below the lower limit for detection (dashed vertical line).

We explore the effect of a threshold further by measuring the mean mass surface densities, $\langle\Sigma\rangle$, for our sample of simulated clouds assuming five possible extinction thresholds ($A_{V,\rm th}$ (mag) = 0.5, 1.0, 1.5, 4, 8) and comparing them to the mean mass surface densities of observed molecular clouds. Only pixels with column densities above a given threshold contribute to estimates of $\langle\Sigma\rangle$. Using near-IR extinction observations of molecular clouds, Lombardi et al. (2010) measured $\langle\Sigma\rangle$ for five different K-band extinction thresholds: $A_{K,\rm th}$ = [0.1, 0.2, 0.5, 1.0, 1.5] ($A_K/A_V = 0.11$; Rieke & Lebofsky, 1985) and found that different clouds will have a constant column density for a given threshold and the value of the column density is dependent on the threshold. Fig. 3.7 shows the agreement between our results (black stars) and the observational estimates of $\langle\Sigma\rangle$ by Lombardi et al. (2010) (black dots) along with their corresponding fit, $\Sigma = 265$ M$_\odot$ pc$^{-2}(A_{\rm th}/{\rm mag})^{0.8}$ (black dashed line). The most

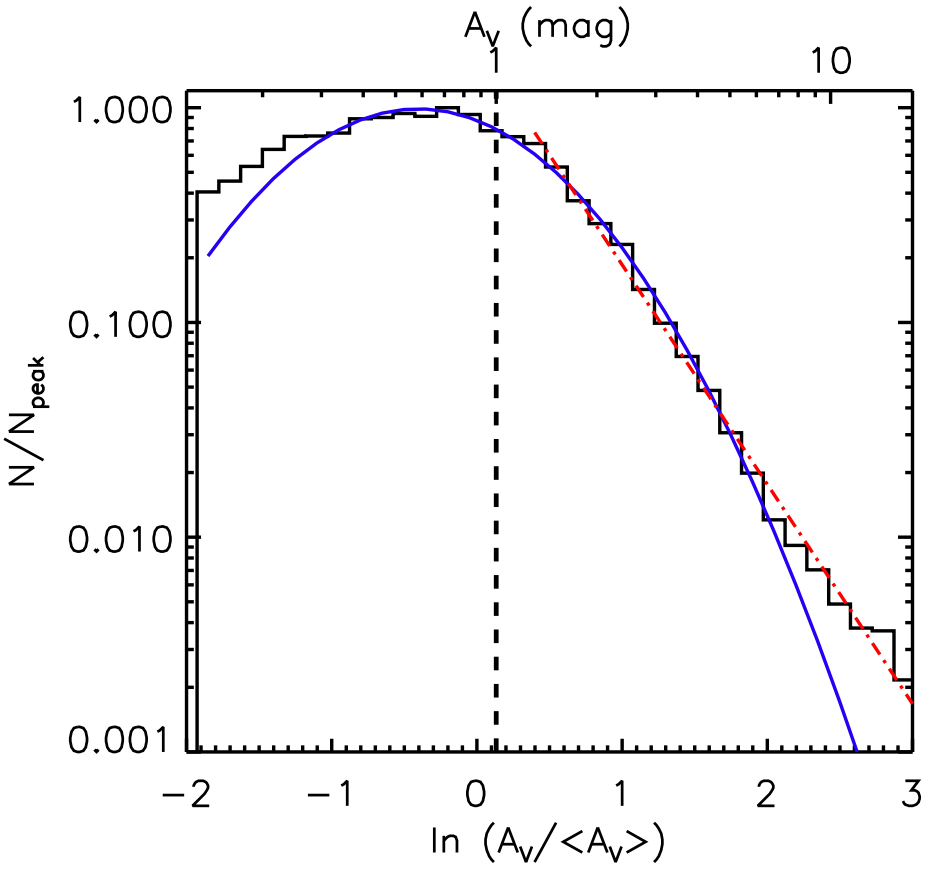

Figure 3.6 Column density PDF for a sample cloud at a late stage of its evolution ($t > t_{\rm ff}$). The solid line shows the lognormal fit to the distribution and the dash-dotted line shows the power-law fit to the tail of the distribution. The dashed vertical line at $A_V = 1$ mag represents the lower limit for detection adopted by Lombardi et al. (2014).

recent estimates for mean surface densities of nearby clouds from Schneider et al. (2014) are also shown (red circles).

Lombardi et al. (2010) argue that their results are a consequence of cloud structure described by a lognormal column density PDF. However, Beaumont et al. (2012) and Ballesteros-Paredes et al. (2012) both suggest that alternate forms of the column density PDF could also produce these results provided that the chosen thresholds are near or above the peak of the distribution. In particular, Ballesteros-Paredes et al. (2012) explored the consequences of several different functional forms of the column density PDF. While they argue that the results of Lombardi et al. (2010) are an effect of thresholding the surface density, their analytic models do show that a lognormal column density PDF with or without a power-law tail can fit the observations. In Fig. 3.7, we plotted six possible cases of their model for a lognormal-shaped column density PDF, shown as grey lines, where

$$\begin{aligned}\langle\Sigma(A_{V,\mathrm{th}})\rangle = (17.5\,\mathrm{M}_\odot\,\mathrm{pc}^{-2})A_{\mathrm{peak}}\exp\left(\frac{\sigma^2}{2}\right)\\ \times\frac{1-\mathrm{erf}\{[\ln(A_{V,\mathrm{th}}/A_{\mathrm{peak}})-\sigma^2]/\sqrt{2}\sigma\}}{1-\mathrm{erf}[\ln(A_{V,\mathrm{th}}/A_{\mathrm{peak}})/\sqrt{2}\sigma]}\end{aligned} \tag{3.2}$$

(Ballesteros-Paredes et al., 2012) with $A_{\mathrm{peak}} = 1$ mag (shown as solid lines) or $A_{\mathrm{peak}} = 0.3$ mag (shown as dash-dotted lines) and $\sigma = 0.6$, 0.9, and 1.2 for the widths of each A_{peak} distribution. We find that a lognormal distribution is consistent with both the observational data of Lombardi et al. (2010) and our simulated clouds. The analytic solutions plateau for extinction thresholds less than the peak for the $A_{\mathrm{peak}} = 1$ mag case. However, once the peak of the distribution evolves to lower surface densities (and correspondingly lower

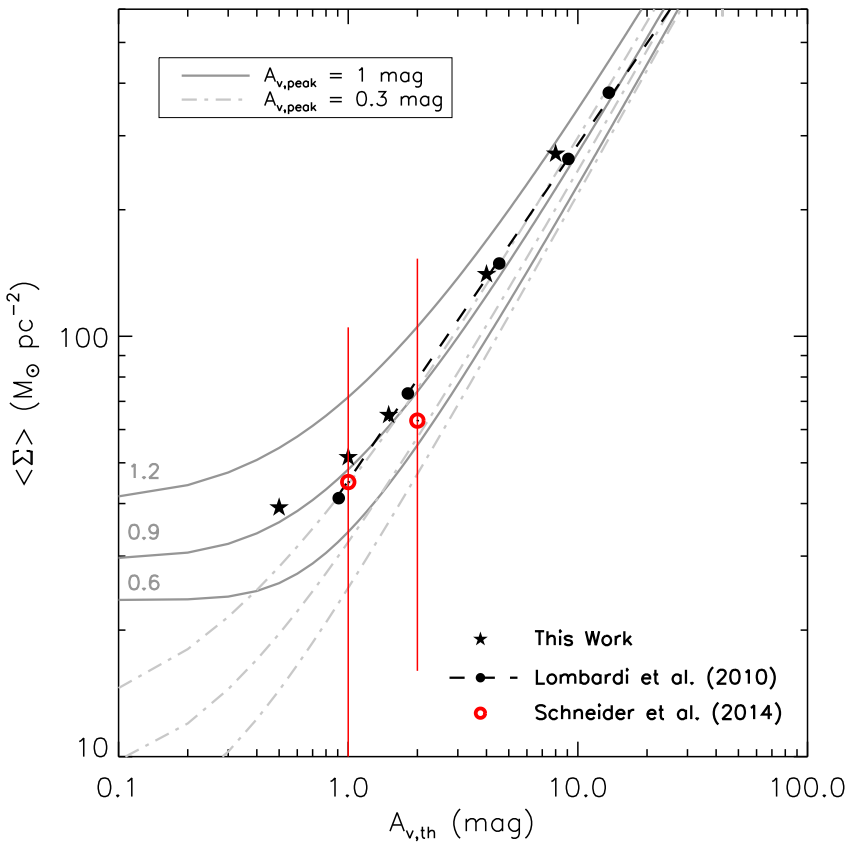

Figure 3.7 Mean mass surface density as a function of the threshold, given by the corresponding extinction threshold, $A_{V,\mathrm{th}}$. The black stars represent the mean mass surface densities of our sample of simulated molecular clouds for five thresholds corresponding to $A_{V,\mathrm{th}}$ = [0.5, 1, 1.5, 4, 8]. The black dots represent the mean mass surface densities for a sample of *observed* clouds obtained from table 1 of Lombardi et al. (2010). The black dashed line is a power-law fit to the observed data from Lombardi et al. (2010). The grey lines are analytic calculations of the mean surface density as a function of the threshold assuming a lognormal column density probability distribution function (PDF) with a peak at $A_{V,\mathrm{peak}}$ = 1 mag (solid line) and at $A_{V,\mathrm{peak}}$ = 0.3 mag (dash-dotted line) and standard deviations of σ = [0.6, 0.9, 1.2] (Lombardi et al., 2010; Ballesteros-Paredes et al., 2012).

extinctions) such as for the $A_{\rm peak} = 0.3$ mag case, the mean surface density is always a function of the threshold across the entire range of threshold values.

We have shown that due to the peaked distribution of the column density PDF, great care must be taken when determining the mean mass surface density as the estimate depends sensitively on the choice of threshold. Clouds disperse as they evolve, resulting in localised high density regions within a cloud dominated by low-density molecular gas. Provided that the threshold is below or near the peak of the distribution, the measure of mean cloud mass surface density can be trusted; however at late times, many of the cloud properties, including the mass and area, will be largely underestimated as they now have evolved to become a function of the threshold.

Cloud dispersal can also lead to a wider lognormal surface density PDF. This widening, seen in Fig. 3.5(b), is expected for clouds with increasing Mach numbers (see section 3.4) and is in agreement with Ballesteros-Paredes et al. (2011) and Tassis et al. (2010) who have shown that the distribution will widen prior to the development of a power-law tail.

The power-law tail is an interesting feature of the column density PDF. Many authors (e.g. Tassis et al., 2010; Ballesteros-Paredes et al., 2011; Kritsuk et al., 2011) have shown that the development of a power-law tail occurs as the cloud evolves from being turbulence-dominated to being gravity-dominated. However, there is still a question as to whether or not the slope of the tail is universal. Froebrich et al. (2007) attribute a variation in the slope to cloud distance based on 2MASS observations of molecular clouds. Ballesteros-Paredes et al. (2011) also argue against a universal slope as they find variation due to projection in their simulations of clouds formed at the interface of colliding

streams. However, neither of these interpretations account for cloud age and evolution.

In Fig. 3.5(c), we show the slopes of the power-law tails obtained from the column density PDFs of our simulated clouds as a function of time. At early times, the slopes are very steep, as they coincide with the lognormal fits at high column densities. As the clouds evolve, the slopes become more shallow, eventually converging to a power-law slope of approximately -2. This result is in agreement with Kritsuk et al. (2011) who also do not see large variation in their power-law slopes with a range of values between -2.8 and -2. Previous studies which have found power-law tails with varying slopes are consistent with our findings for clouds at early stages of their evolution, but our results show that the slopes trend towards a constant value at late times. A universal slope for the high-mass end of molecular cloud structure is appealing as it links the column density distribution of the gas to the initial mass function (IMF) of stars. However, this slope is largely dependent on the point, $\Sigma_{\rm tail}$, where the tail begins its divergence from the lognormal distribution. Determining whether or not the deviation point is constant will aid in our understanding of the universality of the slope and its relation to star formation.

Fig. 3.5(d) shows the evolution of the deviation point as a function of time. We find a decreasing trend towards constant values of the deviation point, consistent with observations (Kainulainen et al., 2011; Schneider et al., 2014). The reason for this is that the peak of the distribution is also changing with time (Fig. 3.5(a)). As the distribution widens, the peak shifts to lower extinction values, resulting in a relatively constant transition point at $A_{V,\rm tail} \sim 4$ mag for the power-law tail at late times. This deviation point is

consistent with the value estimated from 2MASS observations by Kainulainen et al. (2011, $A_{V,\mathrm{tail}} \approx 2 - 4$ mag) and from *Herschel* observations by Schneider et al. (2014, $A_{V,\mathrm{tail}} \approx 4 - 5$ mag). Once gravity begins to dominate, the tail deviates from the lognormal and grows to have a shallower slope. The peak of the distribution is simultaneously decreasing so, by the time star formation takes hold, the dense gas component is entirely confined to the tail of the distribution for surface density values greater than a constant deviation point of $A_{V,\mathrm{tail}} > 4$ mag.

Lada et al. (2010) define an extinction threshold for star formation, above which the surface density of the participating gas correlates linearly with the star formation rate. The authors assume that the material at visual extinctions of greater than 7.3 mag corresponds to a gas volume density of 10^4 cm^{-3} (Bergin et al., 2001). Heiderman et al. (2010) also found the presence of a star formation threshold in an independent study of young stellar objects (YSOs) using the *Spitzer* c2d and Gould Belt surveys; however, this threshold was at a higher visual extinction of 8.6 mag. Both of these estimates of the star formation threshold are greater than the value of the deviation point found in this work and by other authors (Kainulainen et al., 2011; Schneider et al., 2014); however, $A_{V,\mathrm{tail}}$ by its construction is dominated by the diffuse component of the underlying lognormal PDF. Kainulainen et al. (2011) argue that the surface density where the contribution from the tail dominates more than 90% of the PDF is a more direct comparison to the star formation thresholds. Since we know the volume density of the gas particles in our simulation, we can determine where the dense component of the gas is dominant in our clouds. In Fig. 3.8, we compare the mass in high volume density regions to the mass

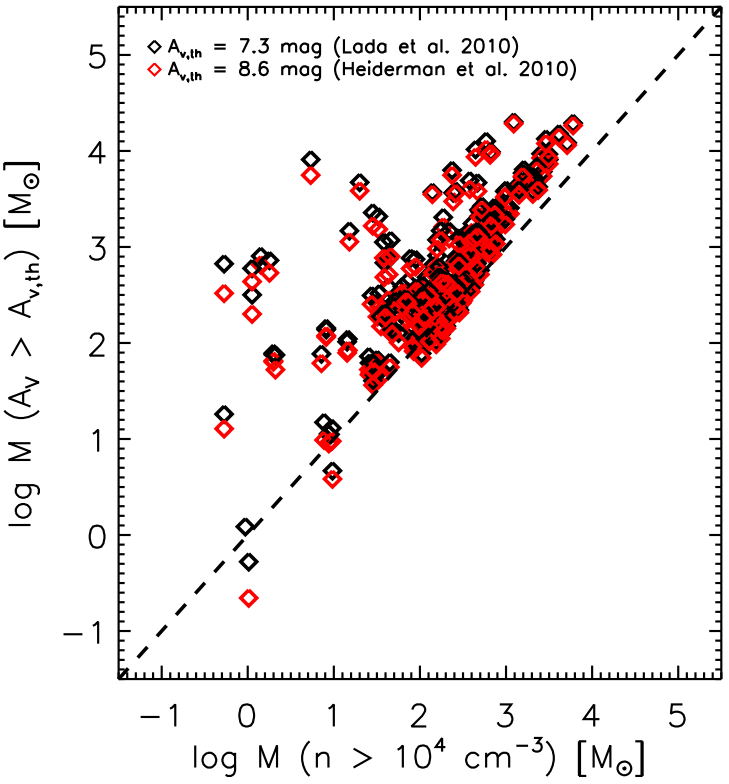

Figure 3.8 Mass found in dense gas ($n > 10^4$ cm^{-3}) compared to the mass found above an extinction of $A_V = 7.3$ mag (black diamonds) or $A_V = 8.6$ mag (red diamonds). The one-to-one line is also shown as a black dashed line.

found at high extinction in our own synthetic maps for the two estimates of the star formation threshold.

This figure shows that masses derived from column density maps will be largely overestimated if one assumes that the star formation threshold is an effective tracer of the dense gas regions corresponding to active star formation. We note however, that while in both cases we find that the mass in high extinction gas is much greater than the mass in high density gas, there still appears to be a correlation, particularly for masses greater than 10^3 M$_\odot$. As

the clouds evolve, the mass in dense gas increases and eventually collapses to form stars. This would explain why the correlation is much tighter at higher masses, as it corresponds to later stages of cloud evolution when the cloud begins to actively form stars. This correlation also suggests that we should expect a similar relation as that found by Lada et al. (2010), where the star formation rate (SFR) scales as a function of the mass of high extinction material such that,

$$\text{SFR } (\text{M}_\odot \text{ yr}^{-1}) = 4.6 \pm 2.6 \times 10^{-8} M_{A_V>7.3} \text{ (M}_\odot) \tag{3.3}$$

We calculated the star formation rate for our simulated clouds by dividing the total mass in stars at each output by the total time elapsed since the beginning of the simulation. Fig. 3.9 shows the SFR in our clouds as a function of the cloud mass above the extinction threshold $A_V = 7.3$ mag.

We find that the star formation rate of molecular clouds correlates very well with the mass above a visual extinction of 7.3 mag. We find the best fit to our data is SFR = 10.7×10^{-8} $\text{M}_{A_V>7.3}$, where the coefficient is a factor of approximately 2 larger than that found by Lada et al. (2010). This could be due to a higher star formation efficiency in our simulations than for the observed clouds. Nevertheless, the existence of the correlation confirms the relation between the mass in dense gas and the mass at high extinction as well as the significance of a constant star formation threshold. The evolution towards a constant deviation point is the result of the interplay between all other structural properties of the column density PDF. A constant value for the deviation point at late times leads to a universal slope of the power-law tail: structural properties which are directly linked to the star formation threshold and slope of the high-mass end of the IMF, respectively.

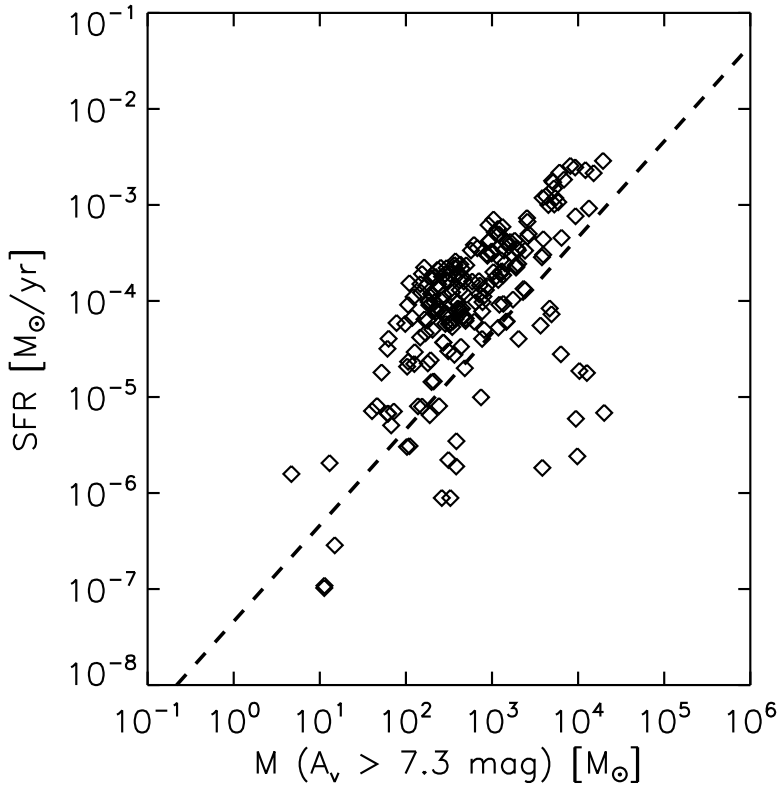

Figure 3.9 Star formation rate as a function of mass above an extinction threshold of $A_V = 7.3$ mag. The best fit to the observations found by Lada et al. (2010) is also shown as a dashed line.

3.4 Conclusions

In this paper, we studied the evolution of the column density PDF of molecular clouds using simulations and synthetic column density maps. For bound and unbound clouds which form from a variety of initial conditions, we find that the column density PDF is consistently represented by a lognormal distribution at early times ($t < 0.25\ t_{\rm ff}$) with a structural transition to a lognormal + power-law tail at late times ($t > 0.5\ t_{\rm ff}$). The evolution of the four key structural properties (σ, $\Sigma_{\rm peak}$, m, and $\Sigma_{\rm tail}$) were explored in detail.

We found that, as a cloud evolves, the peak of its column density PDF will shift to lower extinction values as the distribution widens regardless of whether or not it is gravitationally bound. This means that the underlying lognormal distribution, which can be present for a cloud at early times, will be lost for that same cloud at late times due to the evolution of the peak below the observational threshold for detection. Our results help to explain why certain observations of actively star-forming, dynamically older clouds, such as the Orion molecular cloud, do not appear to have any evidence of a lognormal distribution in their column density PDFs and are instead represented by a power-law tail over the full range of extinction (Lombardi et al., 2014). We also find an increase in the column density variance, even though we do not have externally driven turbulence in our simulations. Therefore, the widening of the distribution does not depend solely on the supersonic turbulence (see also Tassis et al., 2010), but arises as a result of density perturbations produced by localised gravitational collapse.

By studying the evolution of the slope and deviation point of the power-law tails for our sample of simulated clouds, we also show that the range for both properties narrows as they trend towards constant values, thus linking the column density structure of the molecular cloud to such stellar properties as the initial mass function and the surface density threshold for star formation. Although the mass in high extinction gas is much greater than the mass in dense gas, we still find a correlation between the two, particularly at masses greater than 10^3 $M_\odot$. We also show that the thresholds used to define the minimum surface density of gas participating in star formation (Heiderman et

al., 2010; Lada et al., 2010) are suitable tracers of the star formation rates in molecular clouds.

A study of the statistics of cloud properties for a large population of molecular clouds formed in a galactic disc will be the subject of future work. This study will allow for a comparison of our results to clouds observed in galactic and extragalactic environments, as well as further explore the implications of a constant star formation threshold on the star formation rates of bound and unbound molecular clouds.

3.5 Acknowledgments

We would like to thank SHARCNET (Shared Hierarchical Academic Research Computing Network) and Compute/Calcul Canada, which provided dedicated resources to run these simulations. This work was supported by NSERC. J.W. acknowledges support from the Ontario Early Researcher Award (ERA).

Bibliography

Ballesteros-Paredes, J., Vázquez-Semadeni, E., Gazol, A., et al. 2011, MNRAS, 416, 1436

Ballesteros-Paredes, J., D'Alessio, P., & Hartmann, W. L. 2012, MNRAS, 427, 2562

Bate, M. R. & Bonnell, I. A. 2005, MNRAS, 356, 1201

Beaumont, C. N., Goodman, A. A., Alves, J. F., et al. 2012, MNRAS, 423, 2579

Bergin, E. A., Ciardi, D. R., Lada, C. J., Alves, J., & Lada, E. A. 2001, ApJ, 557, 209

Bohlin, R. C., Savage, B. D., & Drake, J. F. 1978, ApJ, 224, 132

Chabrier, G. 2003, PASP, 115, 763

Federrath, C., Banerjee, R., Clark, P. C., & Klessen, R. S. 2010, ApJ, 713, 269

Froebrich, D., Murphy, G C., Smith, M. D., Walsh, J. & del' Burgo, C. 2007, MNRAS, 378, 1447

Goodman, A. A., Pineda, J. E., & Schnee, S. L. 2009, ApJ, 692, 91

Heiderman, A., Evans, N. J., Allen, L. E., Huard, T., & Heyer, M. 2010, ApJ, 723, 1019

Hennebelle, P. & Chabrier, G. 2008, ApJ, 684, 395

Kainulainen, J., Lada, C. J., Rathborne, J. M., & Alves, J. F. 2009, A&A, 497, 399

Kainulainen, J., Beuther, H., Banerjee, R., Federrath, C., & Henning, T. 2011, A&A, 530, A64

Kainulainen, J., Federrath, C., & Henning, T. 2013, A&A, 553, 8

Kritsuk, A. G., Norman, M. L., & Wagner, R. 2011, ApJ, 727, L20

Kroupa, P. 2001, MNRAS, 322, 231

Krumholz, M. R. & McKee, C. F. 2005, ApJ, 630, 250

Lada, C. J., Lombardi, M., & Alves, J. F. 2010, ApJ, 724, 687

Lombardi, M., Alves, J., & Lada, C. J. 2010, A&A, 519, 7

Lombardi, M., Bouy, H., Alves, J., & Lada, C. J. 2014, A&A, 566, A45

Nordlund, Å. & Padoan, P. 1999, Interstellar Turbulence, ed. J. Franco & A. Carraminana, 218

Nutter, D., Kirk, J. M., Stamatellos, D., & Ward-Thompson, D. 2008, MNRAS, 384, 755

Ostriker, E. C., Stone, J. M., & Gammie, C. F. 2001, ApJ, 546, 980

Padoan, P. & Nordlund, Å. 2002, ApJ, 576, 870

Rieke, G. H. & Lebofsky, M. J. 1985, ApJ, 288, 618

Salpeter, E. E. 1955, ApJ, 121, 161

Schneider, N., Ossenkopf, V., Csengeri, T., et al. 2014, submitted (arXiv:1403.2996)

Tassis, K., Christie, D. A., Urban, A., et al. 2010, MNRAS, 408, 1089

Vázquez-Semadeni, E. 1994, ApJ, 423, 681

Wadsley, J. W., Stadel, J., & Quinn, T. 2004, New Astronomy, 9, 137

Ward, R. L., Wadsley, J., Sills, A., & Petitclerc, N. 2012, ApJ, 756, 119

Ward, R. L., Wadsley, J., & Sills, A. 2014, MNRAS, 439, 651

Chapter 4

The Properties of Bound and Unbound Molecular Cloud Populations Formed in Galactic Disc Simulations

Rachel L. Ward, Samantha M. Benincasa, James Wadsley, Alison Sills, & H. M. P. Couchman *2015, MNRAS submitted*

Abstract

We explore the effect of galactic environment on properties of molecular clouds. Using clouds formed in a large-scale galactic disc simulation, we measure the observable properties from synthetic column density maps. We confirm that a significant fraction of unbound clouds forms naturally in a galactic disc environment and that a mixed population of bound and unbound clouds can match observed scaling relations and distributions for extragalactic molecular clouds. By dividing the clouds into inner and outer disc populations, we compare their distributions of properties and test whether there are statistically significant differences between them. We find that clouds in the outer disc have lower masses, sizes, and velocity dispersions as compared to those in the inner disc for reasonable choices of the inner/outer boundary. We attribute the differences to the strong impact of galactic shear on the disc stability at large galactocentric radii. In particular, our Toomre analysis of the disc shows a narrowing envelope of unstable masses as a function of radius, resulting in the formation of smaller, lower mass fragments in the outer disc. We also show that the star formation rate is affected by the environment of the parent cloud, and is particularly influenced by the underlying surface density profile of the gas throughout the disc. Our work highlights the strengths of using galaxy-scale simulations to understand the formation and evolution of cloud properties – and the star formation within them – in the context of their environment.

4.1 Introduction

Stars form principally, and possibly exclusively, in giant molecular clouds (GMCs) which are large conglomerations of gas and dust, predominantly composed of molecular hydrogen and concentrated in the arms of spiral galaxies. With the advent of powerful new telescopes like ALMA with the ability to reach previously unprecedented resolutions, it is now possible to study local clouds in greater detail than ever before. However, limited information can be obtained on the internal structure of extragalactic GMCs from observations of nearby galaxies as they typically have cloud-scale resolution. Observers can partially overcome this limitation by combining data from various surveys to probe the multi-phase ISM and trace star formation throughout a galaxy. There have been several multi-wavelength surveys in recent years (e.g. Rosolowsky et al., 2007; Bigiel et al., 2008; Schinnerer et al., 2013) which have mapped the gas, dust, and stellar distribution of several nearby galaxies, including M31 and M33. Multi-wavelength studies can identify the relationship between stars and the surrounding molecular gas, and reveal whether the relations present at small scales locally, such as the Larson (1981) scaling relations often used to describe local clouds, also exist on larger scales.

The empirical scaling relations of Larson (1981) are considered to be integral to our understanding of the fundamental nature of molecular clouds as they link three key properties which define cloud structure: the mass, size, and velocity dispersion. However, in cases where observations achieved great sensitivity and high resolution, such as the study by Heyer et al. (2009), molecular clouds were found to span a wide range of surface densities, in contrast with the near constant surface densities measured by Larson (1981). Lombardi et

al. (2010) concluded that the surface density for molecular clouds required to satisfy Larson's scaling relations is only constant for a given detection threshold, and the value of the surface density is a function of that threshold.

Due to the varying surface density of molecular clouds, several authors (e.g. Ward et al., 2014; Heyer et al., 2009) are now examining their clouds with respect to the relation between the size-linewidth coefficient, $v_o = \sigma/R^{1/2}$, and the surface density, Σ. The v_o-Σ scaling relation delineates populations of clouds which are bound, unbound, or in virial or pressure-bounded equilibrium (Ballesteros-Paredes et al., 2011; Field et al., 2011; Heyer et al., 2009). This relation allows us to better understand the internal structure and dynamics of molecular clouds as well as the nature of the ISM environment in our own Galaxy.

The v_o-Σ relation can also guide our understanding of clouds in an extragalactic context, such as in the examination of the relation on global scales in a recent study by Leroy et al. (2015) who use the relation to compare populations of clouds in different environments for several nearby galaxies. The authors find that many of the GMCs in the Milky Way and in nearby galaxies that satisfy the scaling relation are in virial equilibrium without external pressure confinement; however, there is significant scatter in the data indicating that some of the clouds in these galaxies could be marginally unbound. The clouds which are highly unbound were those in the Galactic centre and in the outer disc of the Milky Way, which suggests that environment has an effect on the virial state of molecular clouds. The effect of the environment on the structure and evolution of molecular clouds will be explored throughout this work.

In this paper, we explore the properties of clouds formed in a simulated galactic disc. We investigate how the formation and evolution of these clouds and their stars are affected by their environment. Using clouds identified from synthetic column density maps, we compare the Larson and v_o-Σ scaling relations and distributions of properties for our cloud populations to observations of molecular clouds in nearby galaxies. By studying the simulated cloud populations with respect to their location in the disc, we can determine whether the environment, particularly the galactic shear rate, affects the global properties of molecular clouds and star formation.

In section 4.2, we describe the details of the simulation and the methods by which the synthetic observations were produced and the clouds were identified. In section 4.3, we present our results and conclude with a summary and discussion on the implications of our findings in section 4.4.

4.2 Methods

Using the smoothed particle hydrodynamics (SPH) code GASOLINE (Wadsley et al., 2004), we simulated a large-scale galactic disc. The model we adopt is similar to the models of Tasker & Tan (2009), Tasker (2011), and Dobbs et al. (2011b), and includes a static galactic potential, self-gravity, mechanisms for heating and cooling, star formation, and stellar feedback. The disc properties are summarized in Table 4.1. The total gas mass in the simulation is of the same order as that in the Milky Way and the spiral galaxy M33 (Corbelli & Salucci, 2000). The overall global properties of our disc, including the molecular gas surface density (when $n > 100$ cm^{-3}) and galactic shear, are also well-matched to those for M33 (Corbelli & Salucci, 2000; Heyer et al.,

2004). We used the same logarithmic dark matter halo potential as Tasker & Tan (2009) and Dobbs et al. (2011b) to produce an approximately flat rotation curve, typical of observed spiral galaxies and described by the rotational velocity of the galactic disc,

$$v = \Omega R_{\rm gal} = \frac{v_{\rm c} R_{\rm gal}}{\sqrt{R_0^2 + R_{\rm gal}^2}}, \tag{4.1}$$

(Binney & Tremaine, 2008) where $v_{\rm c} = 220$ km s^{-1} is the constant rotational velocity at large radii chosen to be comparable to the Milky Way rotational velocity at the solar radius (8 kpc). When $R_{\rm gal} \gg R_0 = 1$ kpc, the rotational velocity is constant at $v = v_{\rm c}$. The disc was initialised with a Kolmogorov turbulence spectrum, producing random velocity perturbations in the x, y, and z directions. The resulting surface density profile of the disc is truncated between 12 and 14 kpc and normalized to 14 M$_\odot$ pc^{-2} at the solar radius. We also excluded the dense, compact centre of the galaxy ($R_{\rm gal} < R_0$) to conserve resolution in our simulation. We use the stochastic star formation criteria outlined in Stinson et al. (2006) to determine whether a gas particle of mass $m_{\rm gas}$ is eligible to be converted into a star particle, which in our case represents a cluster of stars with mass $m_{\rm star}$ determined by a core-to-star efficiency factor of 30% (e.g. Lada & Lada, 2003). To determine the probability that a star will form, we use a constant galactic star formation efficiency per dynamical time, c_*, of 6%, which is typical for cosmological and galactic disc simulations (e.g. Stinson et al., 2006; Governato et al., 2007; Tasker & Bryan, 2008). We adopt a stellar feedback prescription based on the model proposed by Agertz et al. (2013), where supernovae feedback energy is deposited to the ISM via the nearest gas particle to the star and is converted from a non-cooling state to a radiative cooling form of energy over a timescale of 5 Myr (see also Keller

Table 4.1 Properties of the global galactic disc simulation

Gas mass	7.5×10^9 $M_\odot$
Radius	15 kpc
Mass resolution, $m_{\rm gas}$	441 $M_\odot$
Σ(r = 8 kpc)	14 $M_\odot$ pc^{-2}
Scale height	300 pc
Star formation efficiency, c_*	6 %
Feedback efficiency	10 %

et al., 2014, Benincasa et al. 2015, in preparation). We explore a case where 10% of the total feedback energy is available to be delivered throughout the disc, corresponding to 10^{50} erg of energy.

We used synthetic column density maps of the entire galactic disc to compare our results more directly to observations. To create these maps, we interpolated the SPH particles onto a 5000 × 5000 grid using a kernel function (Monaghan & Lattanzio, 1985) similar to the method of Ward et al. (2012). Each map has a grid spacing of 6 pc, which was chosen to match the 1.″5 resolution of the M33 observations made by Rosolowsky et al. (2003). The gravitational softening length is 20 pc with a minimum smoothing length of 10 pc. By smoothing our column density map using a Gaussian, we can match the effective resolution of observations by selecting a full-width half-maximum (FWHM) equal to the beam width of a given telescope while also ensuring that our resolution is greater than our softening. As a result, our surface density maps have an effective spatial resolution of 24 pc.

In our analysis, the individual SPH particles must satisfy the condition that their densities are greater than 100 cm^{-3}, corresponding to the threshold

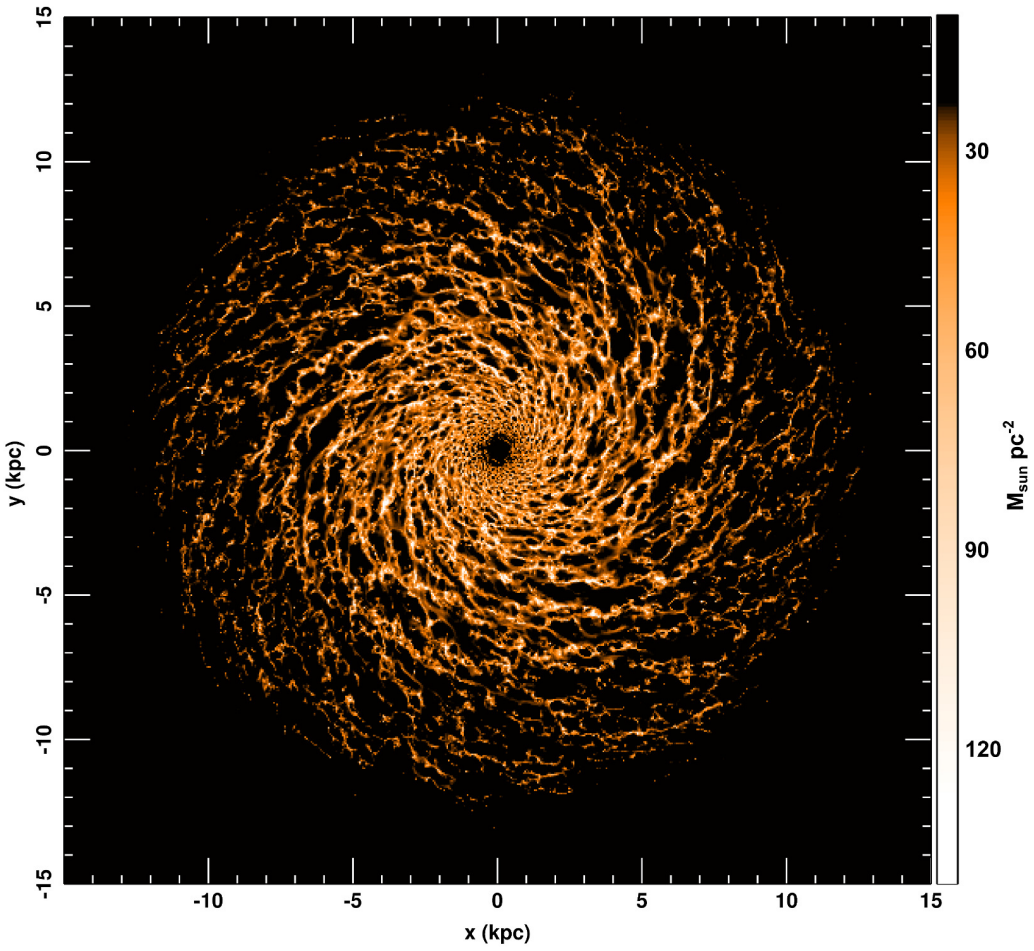

Figure 4.1 – Synthetic column density map of a galactic disc at 500 Myr. The map shows the gas with surface density above a threshold of 10 $M_\odot$ pc^{-2}.

density to form molecular hydrogen. The synthetic column density map is shown in Figure 4.1.

We identified clouds in our disc using the two-dimensional CUPID implementation of the source extraction algorithm, Clumpfind (Williams et al., 1994), in the Starlink software environment[1]. The clouds are selected using a surface density threshold of ~ 10 M$_\odot$ pc^{-2} and require a minimum number of 7 pixels. This surface density threshold is estimated from the off-source background and is approximately twice the value of the equivalent rms surface density, $\sigma_{\rm rms}$, used by Rosolowsky et al. (2003). Each contour interval was equal to approximately $3\sigma_{\rm rms}$. Clouds that did not extend above the second contour level and clouds with sizes smaller than the effective beam width were rejected. To account for the added smoothing, the deconvolved cloud sizes were recorded. Also, since our mass resolution is ~ 440 M$_\odot$ per particle, we define our completeness limit at 4.4×10^4 M$_\odot$, as clouds with masses below this limit will be resolved by less than 100 particles.

4.3 Results

We examined the properties of molecular clouds identified in our disc at early (250 Myr) and late (500 Myr) times. These times represent approximately one and two rotations of the outer disc, respectively. From the maps, we measured the area, A, and gas mass, M, of each cloud above the surface density threshold. We then calculated the radius of each cloud assuming spherical geometry such that $R = (A/\pi)^{1/2}$. The velocity dispersions determined for each cloud were calculated based on the mass-weighted velocities of the

[1] http://starlink.jach.hawaii.edu

particles assigned to that cloud. Particles with $n > 100$ cm^{-3} were assigned to clouds if their line-of-sight positions intersected with pixels belonging to a given cloud. We used one-dimensional velocity dispersions, $\sigma_{\rm v}$, for our clouds to compare with the line-of-sight velocity dispersions measured in observations. Using the observable properties of mass, radius, and velocity dispersion, we calculated the virial parameter,

$$\alpha = \frac{5\sigma_{\rm v}^2 R}{GM}, \tag{4.2}$$

(Bertoldi & McKee, 1992) which describes simple virial equilibrium where $\alpha = 1$ for virialised clouds and clouds with $\alpha \leq 2$ are gravitationally bound. We also measured properties of the stars, in order to study the star formation with respect to the properties of the clouds in which they form. To determine the star formation rate (SFR) for each cloud, we assigned each star particle to the cloud they coincide with along the line-of-sight. We then calculated the total mass of the stars per cloud and divided by the output time. The star formation rate surface density, $\Sigma_{\rm SFR}$, is calculated by dividing the SFR by the cloud area. These calculations were done at both output times. The median values and median absolute deviations for these properties are summarized in Table 4.2.

We find that the number of clouds increased with time between 250 Myr and 500 Myr and that $\sim 30\%$ of clouds were unbound, demonstrating that a substantial fraction of unbound clouds form naturally in our disc (see also Dobbs et al., 2011a,b; Tasker & Tan, 2009). We also find that the resultant star formation rate surface densities ($\Sigma_{\rm SFR}$) of clouds in this disc are close to – and slightly lower than – those expected from the Kennicutt-Schmidt relation, which shows that the presence of unbound clouds in our disc helps to match

Table 4.2 Median Properties for Molecular Clouds

	$t = 250$ Myr	$t = 500$ Myr
$N_{\rm clouds}$	1398	1557
M (10^5 M$_\odot$)	1.4 ± 0.6	1.6 ± 0.7
R (pc)	36 ± 5	36 ± 5
$\sigma_{\rm v}$ (km s^{-1})	2.4 ± 0.6	2.5 ± 0.6
$v_o = \sigma_{\rm v}/R^{1/2}$ (km s^{-1} pc$^{-1/2}$)	0.4 ± 0.1	0.4 ± 0.1
α	1.5 ± 0.5	1.5 ± 0.5
Σ (M$_\odot$ pc^{-2})	35 ± 9	40 ± 10
$\Sigma_{\rm SFR}$ (10^{-3} M$_\odot$ yr^{-1} kpc^{-2})	6 ± 3	5 ± 2

Notes: $N_{\rm clouds}$ is the total number of clouds, M is the cloud mass, R is the cloud radius, $\sigma_{\rm v}$ is the one-dimensional velocity dispersion where $3\sigma_{\rm v}^2 = (\sigma_{\rm v_x}^2 + \sigma_{\rm v_y}^2 + \sigma_{\rm v_z}^2)$, v_o is the size-linewidth coefficient, α is the virial parameter where $\alpha = 2$ for clouds in gravitational equilibrium, Σ is the gas surface density, and $\Sigma_{\rm SFR}$ is the star formation rate surface density. The median and median absolute deviation is listed for all cloud properties for direct comparison to the results for M33 provided in Hughes et al. (2013).

the low galactic star formation rates observed in the Milky Way (Robitaille & Whitney, 2010) and nearby galaxies (Kennicutt, 1998; Bigiel et al., 2008).

To understand these results in the context of the formation and interactions of clouds in the disc, we calculated the angular momentum vector for each cloud and determined the angle offset, θ, from the angular momentum vector of the galactic disc. This angle represents the axial tilt of the cloud with respect to the disc. A cloud with $|\theta| < 90^\circ$ is rotating the same direction as the disc, or prograde, and those with $90^\circ < |\theta| < 180^\circ$ are retrograde with respect to the disc. Clouds which form in the disc due to a gravitational instability will inherit the direction of the disc's rotation, resulting in a cloud that is rotating prograde relative to the disc. Therefore, if clouds are found to be rotating retrograde with respect to the disc, we can assume that they have been perturbed by an interaction with the disc or by a collision with another

cloud (Tasker & Tan, 2009). We find that the overwhelming majority of clouds are prograde as expected for clouds forming in a disc environment; however, we do find a significant population (13%) of clouds with retrograde rotation at 250 Myr. The percentage of clouds with retrograde rotations does not increase with time, which suggests that the low amount of energy injection from feedback results in few cloud collisions and interactions over time and more star formation. Since there was little disruption of the disc due to the low feedback energy from stars, clouds were able to form, grow, and evolve.

4.3.1 Comparison to observations

At a distance of 0.84 Mpc (Freedman et al., 1991), M33 is one of the nearest galaxies to the Milky Way which makes it a prime candidate for comparison to our simulations as, not only are its gross properties comparable to the simulation, but its clouds are observationally well resolved at this distance. We identified 1557 molecular clouds in the simulated galactic disc at 500 Myr. In Figure 4.2, we compare the distributions of cloud properties for the simulated clouds (black histograms) to those for 149 real molecular clouds (grey histograms) from multi-wavelength observations of M33 (Rosolowsky et al., 2007). Although the grid spacing and resolution of our synthetic column density maps match the M33 observations of Rosolowsky et al. (2003), the less-resolved sample of observed clouds by Rosolowsky et al. (2007) is more appropriate for comparison as it uses a merged multi-wavelength data set to produce a fully-sampled map of the entire galaxy. The authors find that the majority of the clouds detected lie within a galactocentric radius of 4 kpc, resulting in a number density of approximately 3 clouds kpc^{-2}, consistent with

the number density of clouds in our comparatively larger simulated disc. We find excellent agreement between the observed and simulated cloud distributions for the masses, sizes, and surface densities, as confirmed by a two-sided Kolmogorov-Smirnov (KS) test. The KS test showed statistical differences between the observed and simulated cloud distributions for velocity dispersion and its related properties, v_o and α; however, we see that the medians and ranges of values for these properties in our simulated clouds are similar to those in the observed clouds. These results demonstrate that the global properties of our simulated clouds are comparable to those in M33.

We also find that our clouds lie on the scaling relations of Larson (1981) determined from Galactic molecular cloud data, shown by the dashed black lines in the top left and right panels of Figure 4.3. The scaling relation derived from observations of extragalactic molecular clouds by Bolatto et al. (2008) is also shown as a dot-dashed line in the top right panel for comparison to our results. We find that, although Larson's laws originated from observations of local clouds, the scaling relations are still present on larger scales in our simulations of an extragalactic cloud population. We note however that there is still a lot of scatter in the observed and simulated data. In Ward et al. (2014), we showed that the scatter accompanying the Larson scaling relations for local clouds was attributed to a spread in the cloud surface density, Σ, and the intrinsic virial parameter. We plot the size-linewidth coefficient, v_o, as a function of Σ to determine the spread in the virial parameter at fixed surface density and we see that both the simulated (black points) and observed (grey circles) populations consist of bound and unbound clouds, where gravitationally bound clouds lie below the dashed line where $\alpha = 2$. Based on the results

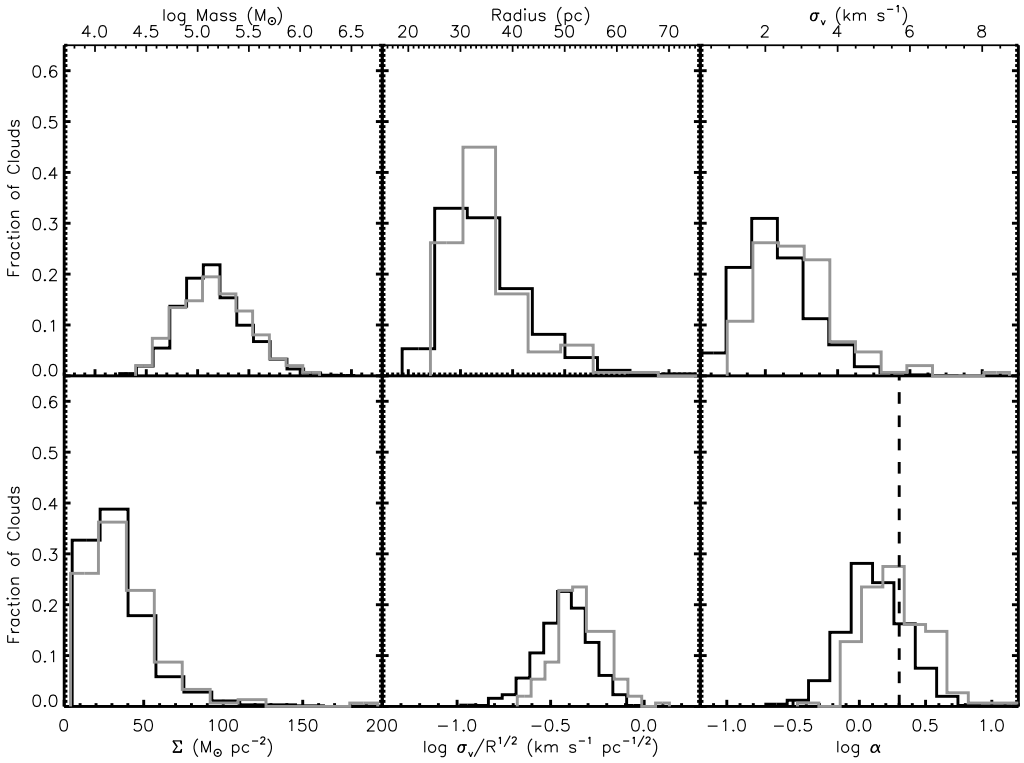

Figure 4.2 – Distributions for the mass, radius, velocity dispersion ($\sigma_{\rm v}$), surface density (Σ), size-linewidth coefficient (v_o), and virial parameter (α) of molecular clouds in our sample (black histograms) with 10% feedback efficiency at 500 Myr. The corresponding distributions for the clouds identified in M33 (Rosolowsky et al., 2007) are shown as grey histograms for comparison. The vertical dashed line in the bottom-right panel represents the boundary to the left of which clouds are gravitationally bound.

of Ward et al. (2014), this is not unexpected as we previously showed that a substantial population of unbound clouds can match the observed scaling relations with their accompanying scatter in addition to forming stars; however, we have now demonstrated that unbound clouds can not only match these observations but they form naturally in a galactic disc environment, under the effects of galactic potential, shear, external pressure, and stellar feedback.

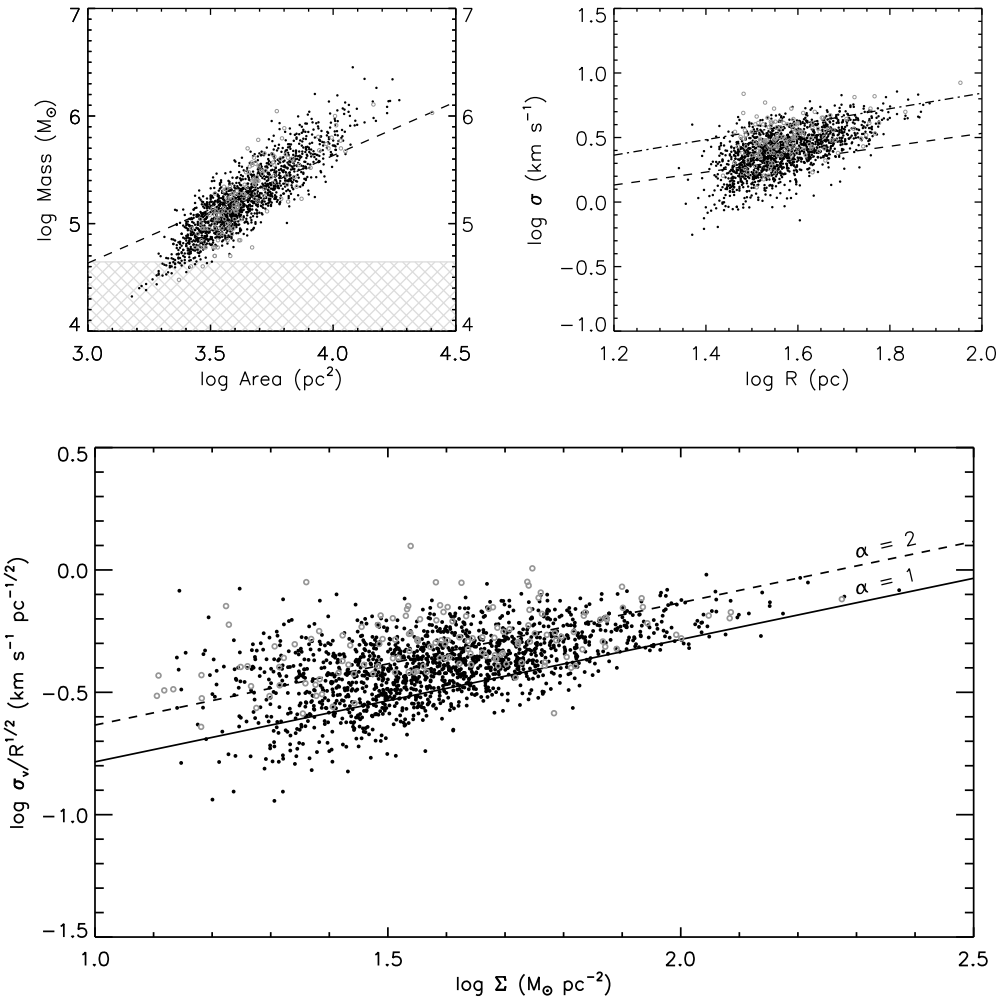

Figure 4.3 – Scaling relations for molecular clouds extracted from synthetic column density maps. Mass as a function of cloud area (top left) and linewidth as a function of cloud radius (top right) are shown with their corresponding empirical scaling relation of Larson (1981) (dashed black lines). Molecular cloud data from observations of M33 by Rosolowsky et al. (2007) are also shown (grey circles). The grey hashed region in the top left panel shows masses for clouds with less than 100 particles. The dot-dashed line in the top right panel shows the scaling relation derived from observations of extragalactic clouds by Bolatto et al. (2008) for comparison. The size-linewidth coefficient, v_o, as a function of the surface density (bottom) is also shown, where the dashed and solid black lines represent the boundaries below which clouds are gravitationally bound ($\alpha = 2$) and virialised ($\alpha = 1$) respectively.

Unbound clouds have been simulated in detail in several recent studies in both isolation (e.g. Clark et al., 2005, 2008; Bonnell et al., 2011; Ward et al., 2014) and in galactic discs (e.g. Dobbs et al., 2011a,b; Hopkins et al., 2012). These studies have shown that there are a number of factors, both internal and external, that can affect the virial parameter of a molecular cloud. High mass clouds tend to be more strongly bound than less massive clouds as seen in the observations of Heyer, Carpenter, & Snell (2001) and the models of Hopkins et al. (2012). Although several authors argue that these low mass clouds must be in pressure-confined virial equilibrium, the necessary pressures to maintain equilibrium for these broadened linewidths can be upwards of 10^7 cm^{-3} K (Field et al., 2011) for some clouds, much higher than the typical ambient ISM pressure of $P/k_{\rm B} \sim 10^{3-4}$ cm^{-3} K (Wolfire et al., 2003). An alternative theory is that some of these clouds are simply unbound and short-lived with lifetimes of $\sim$ 10 - 15 Myr (Clark et al., 2005, and references therein). Molecular clouds can be disrupted by cloud-cloud collisions, galactic shear, and supernovae feedback, all of which are sources of turbulence in the disc. The more turbulent the molecular gas, the 'puffier' the cloud will be for a fixed virial parameter and surface density, as seen in the size-linewidth scaling relation. As noted earlier in this section, turbulence from supernovae feedback and cloud-cloud collisions likely plays an important role in affecting the boundedness and evolution of molecular clouds.

4.3.2 The effect of galactic shear on molecular cloud properties

In addition to turbulence driven by feedback energy and cloud-cloud collisions, turbulence can also arise from shear in the galactic disc. To determine

whether the galactic shear rate, Ω, has a significant effect on the properties of molecular clouds, we divided the cloud population into two regions: the inner galaxy, where the shear rate is high, and the outer galaxy, where the shear rate is much lower. Our choice of the boundary was guided by observations of M33 (Bigiel et al., 2010b; Rosolowsky et al., 2007), where the outer disc of M33 is defined as the region beyond two CO scale lengths ($R_{\rm gal} \approx 4$ kpc). At this radius, the emission has fallen by a factor of e^2. Since our disc is significantly larger than M33, we chose a division based on a matching shear rate rather than galactocentric radius. Using the rotation curve of M33 (Corbelli & Salucci, 2000), we determined that its shear rate at 4 kpc is approximately 27 km s^{-1} kpc^{-1}. An equivalent shear rate in our disc is at a galactocentric radius of approximately 8 kpc, determined using equation 4.1. We sorted each cloud by its location in the disc and produced distributions similar to those shown in Figure 4.2 for the inner (2 – 8 kpc, blue) and outer disc (> 8 kpc, orange), excluding the innermost portion of our disc to avoid any edge effects from the hole in the centre of the model. The distributions were normalized by the number of clouds per distribution and the bin size and are expressed in units of the peak of the inner disc distribution (blue). The resulting distributions are shown in Figure 4.4 for two output times, 250 and 500 Myr.

Figure 4.4 shows that the distributions differ at early and late times for each cloud property. We find that the distributions of properties for clouds in the outer disc with $\Omega < 27$ km s^{-1} kpc^{-1} are shifted to lower masses, sizes, and velocity dispersions. To measure whether there is a statistically significant difference between the distributions of our inner and outer disc cloud properties, we perform a two-sided Kolmogorov-Smirnov (KS) test on

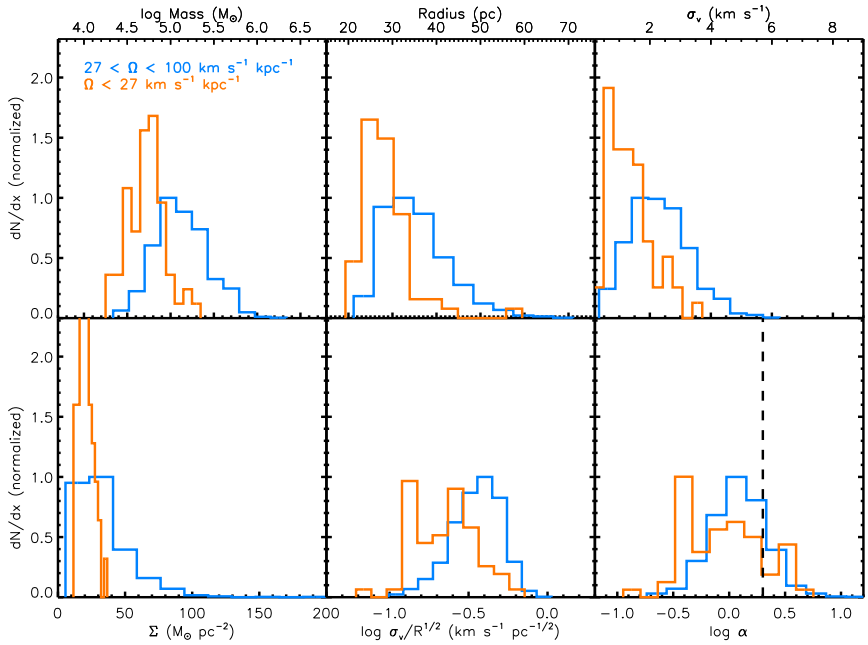

(a) 250 Myr

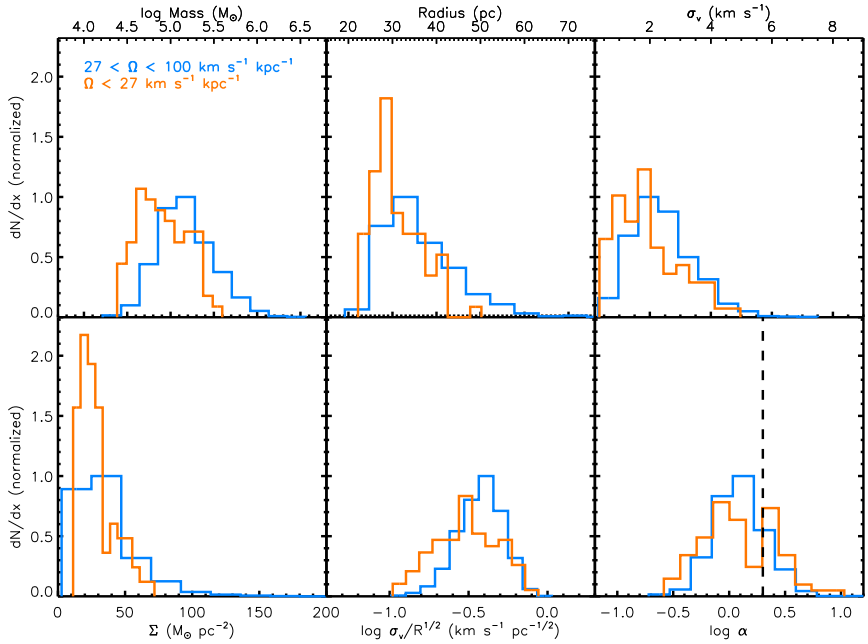

(b) 500 Myr

Figure 4.4 – Cloud properties as described in Figure 4.2 but here the clouds are divided into radial annuli at $R_{\rm gal} = 8$ kpc or equivalently by the differential rotation rate ($\Omega = 27$ km s^{-1} kpc^{-1}) for each annulus.

Table 4.3 KS test probabilities for inner and outer disc molecular clouds

	$t = 250$ Myr	$t = 500$ Myr
M	3.95×10^{-24}	4.13×10^{-12}
R	4.92×10^{-13}	1.18×10^{-10}
$\sigma_{\rm v}$	9.27×10^{-15}	7.89×10^{-8}
Σ	5.64×10^{-24}	5.97×10^{-12}
$v_o = \sigma/R^{1/2}$	5.84×10^{-13}	5.98×10^{-6}
α	3.13×10^{-6}	0.05

the distributions. The probabilities that the inner and outer disc clouds are drawn from the same distribution are given in Table 4.3.

We consider any probabilities, Pr, less than 0.05 an indication that there are statistically significant differences between the distributions. We find that every pair of distributions are statistically different, except for α at 500 Myr which has $Pr = 0.05$. To test the robustness of these results, we permuted the order of the clouds using a pseudorandom number generator and split the data into two distributions in four different ways: 25/75, 50/50, 75/25, and by the fractional amount resulting from a division of the sorted data at a boundary of 8 kpc (95/5). We performed two-sided KS tests on these four pairs of distributions for all properties at both 250 and 500 Myr. We repeated this process 100 times and calculated the mean probabilities that the paired data could be drawn from the same distribution for each cloud property. We found that in every case, regardless of the division of data, all properties had $Pr \gtrsim 0.5$, indicating that it is quite likely that the clouds are similar to one another overall but exhibit distinct statistical differences when they are compared in the context of their environment.

Observations also show that clouds in the outer disc of M33 (Bigiel et al., 2010b) and the Milky Way (Heyer, Carpenter, & Snell, 2001; Brand & Wouterloot, 1995) exhibit lower masses, sizes, and velocity dispersions than those found in the inner disc. These findings are sometimes attributed to low resolution, blending, incomplete sampling, and, for the case of the Milky Way, line-of-sight confusion in the determination of cloud properties in the inner disc. However, we find a real difference between the inner and outer disc cloud populations.

To determine whether our results are dependent on our choice of the boundary, we repeated our statistical comparison of the cloud distributions for the inner and outer disc using the boundary corresponding to one CO scale length or one e-fold of the disc emission, which for M33 is 2.1 kpc (Rosolowsky et al., 2007). Using the shear rate at 2.1 kpc for M33 (Corbelli & Salucci, 2000) and equation 4.1, we calculate the equivalent radius in our disc at this shear rate to be approximately 5.5 kpc. We find similar results as before, although with much less pronounced differences between the inner and outer distributions than those seen for clouds within and beyond the 8 kpc boundary, which indicates that clouds in the farthest reaches of the galaxy are the most strongly affected by environmental factors. Every property still has statistically significant differences with $Pr \ll 0.05$ except for $\sigma_{\rm v}$ and $v_{\rm o}$, which have KS probabilities slightly larger than 0.05 at late times. These results show that, regardless of the boundary, the properties which are most similar over the entire disc are the distributions for the size-linewidth coefficient and the virial parameter, demonstrating that, while the clouds in the inner portion of the disc can have significantly different observable properties from those in the

outer disc, they will still exhibit scaling relations that are consistent regardless of environment.

Rosolowsky et al. (2007) also studied the variation of the cloud mass distributions with galactocentric radius in M33 and found a similar result that the distributions significantly differ for inner and outer disc clouds. In particular, their observations of M33 showed that there were very few molecular clouds in the outer disc beyond 4 kpc, despite the abundance of molecular gas beyond this radius, and that the few clouds found in the outer disc had much lower masses than those within this radius, consistent with our results.

4.3.2.1 Toomre analysis

Molecular clouds appear to be a product of the environment in which they formed; however, it has yet to be determined which environmental factors play a significant role in distinguishing the properties of molecular clouds between the inner and outer disc. Rosolowsky et al. (2007) suggest that cloud properties at small radii could differ due to strong galactic shear and less-defined spiral structure in the region and that the lack of clouds at large radii could be caused by features of the galactic disc, such as its gravitational stability and the surface density distribution of atomic gas. The observable properties (mass, size, and velocity dispersion) are much smaller for clouds formed in the outer disc where the external pressure (Benincasa et al. 2015, in preparation) is weaker. This may seem counter-intuitive as one might expect cloud size to increase with decreased external pressure, but it can be understood if we account for the effect of galactic shear by a Toomre analysis of a differentially rotating disc.

Toomre (1964) considered gravity, thermal pressure, and the Coriolis force caused by rotation the three factors that contribute to the stability of a galactic disc. The Toomre stability criterion which determines the stability boundary at which these factors are balanced is

$$Q = \frac{c_{\rm s}\kappa}{\pi G\Sigma}, \tag{4.3}$$

where κ is the epicyclic frequency, $c_{\rm s}$ is the sound speed, and Σ is the surface density of the disc. If the Toomre Q parameter drops below 1, a differentially rotating disc will be unstable to collapse. To determine the critical wavelength of a perturbation, $\lambda_{\rm crit}$, above which all perturbations are unstable, we must begin with the dispersion relation for a uniformly-rotating fluid disc with a non-zero sound speed,

$$\omega^2 = \kappa^2 - 2\pi G\Sigma|k| + c_{\rm s}^2 k^2, \tag{4.4}$$

(Bertoldi & McKee, 1992) where ω is the oscillation frequency and k is the wave number. By solving for the critical wavenumber, $k_{\rm crit}$, we can then determine the corresponding wavelength, $\lambda_{\rm crit} = 2\pi/k_{\rm crit}$, and subsequently the Toomre mass,

$$M_{\rm T} = \Sigma\lambda_{\rm crit}^2. \tag{4.5}$$

The Toomre mass, $M_{\rm T}$, is analogous to the Jeans mass for the case where the shear rate is an important component to stability. Therefore, we expect regions of the disc unstable against gravitational collapse to form fragments with masses given by the Toomre mass. Since the mass is dependent on the surface density of the disc and the critical wavelength, which are both a function of $R_{\rm gal}$, the mass also scales with the galactocentric radius as shown in Figure 4.5. The solution for the Toomre mass when $\omega = 0$, corresponding

to an infinite timescale for collapse, is shown in Figure 4.5 as a black solid line and represents the line of neutral stability in the disc. Our simulated disc is not pressure-supported ($dP/d\rho < 0$) in the regime where gas densities are ρ = 1 - 10 cm^{-3}, typical for the ISM. Therefore, there is a singular solution to equation 4.4, representing the boundary above which the disc is stable against collapse by galactic shear.

To determine whether there is a characteristic timescale for fragmentation in the disc described by ω, we calculated solutions to equation 4.5 for a range of collapse timescales, $\tau = 1/\omega$, and compared the results to our simulated clouds. While the Toomre mass remained fairly constant throughout the disc when $\tau \to \infty$, as τ decreased, the Toomre mass profile began to decrease more with increasing galactocentric radius and therefore we would expect smaller and lower mass clouds to fragment out of the outer disc. This result supports what we observe in our simulated clouds (shown in Figure 4.5 as black dots) as our population of clouds in the outer disc were found to have lower masses and sizes than those in the inner disc. By confining the cloud data within the envelope of instability created by the solution to equation 4.5, we find that a collapse timescale between 10 and 16 Myr best describes our data with the solutions shown in Figure 4.5 as grey solid lines. We therefore conclude the characteristic formation timescale for clouds in our disc is $\tau_{\rm form} = 13 \pm 3$ Myr. This collapse timescale is comparable to estimates for the lifetime of a molecular cloud within uncertainties (e.g. Murray, 2011; Dobbs et al., 2014), indicating that the formation and destruction of molecular clouds are in approximate equilibrium with one another.

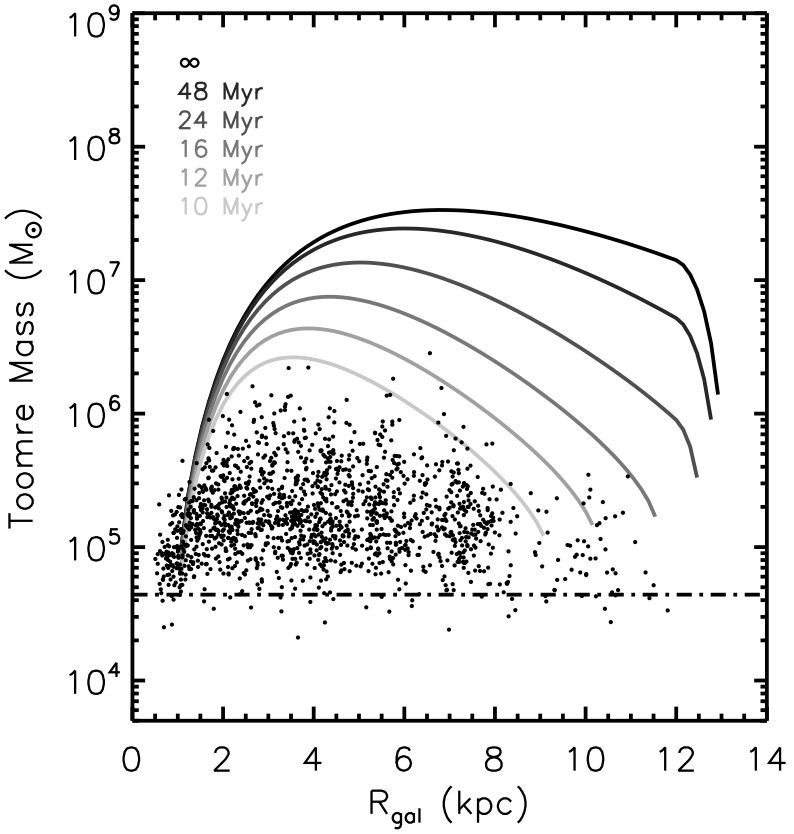

Figure 4.5 – Toomre mass, $M_{\rm T}$, as a function of galactocentric radius. The solid lines represent the boundary above which the disc is supported against collapse by shear and are the solutions to equation 4.5 for six collapse timescales, τ = [∞, 48 Myr, 24 Myr, 16 Myr, 12 Myr, 10 Myr]. The gas masses for clouds identified in our simulated galaxy at 500 Myr are also shown (black dots). The dot-dashed line at 4.4 $\times$ 10^4 $M_\odot$ shows the mass of a cloud resolved by 100 particles.

We find the most significant effect on the properties of the molecular clouds in our disc comes from the galactic shear which causes an overall narrowing envelope of instability at large galactocentric radii, as shown by this Toomre analysis. As we discovered earlier, the properties of clouds in the outer disc will have lower masses and smaller sizes and this result can be understood as

an effect of their environment, due to an increasingly limited range of possible Toomre masses for collapsing gas fragments at large galactocentric radii.

4.3.3 The effect of environment on star formation rate

We found that the environment, particularly the galactic shear rate, can have a significant effect on the gas properties of molecular clouds, but we have not yet explored the effect, if any, it has on the star formation. In Figure 4.6, we show the SFR distribution for clouds in the inner ($2 < R_{\rm gal} < 8$ kpc, blue histogram) and outer disc ($R_{\rm gal} > 8$ kpc, orange histogram).

We find that the SFR is significantly higher in inner disc clouds than it is in outer disc clouds, indicating that the star formation is dependent on the location of their parent cloud in the disc. Figure 4.7 shows the star formation rate surface density ($\Sigma_{\rm SFR}$) as a function of galactocentric radius in the disc and we find a similar profile to the shear-supported boundary for the Toomre mass in Figure 4.5.

We have already shown that the inner disc is populated with larger, more massive clouds, a product of gravitational instabilities resulting from galactic shear. We find that the SFR and the corresponding $\Sigma_{\rm SFR}$ can also be influenced by environmental factors as well, resulting in lower, more inefficient, star formation rates in the outer disc, due to the underlying exponential gas surface density profile of the disc. This relationship between the SFR and the gas surface density is most commonly described using the Kennicutt-Schmidt star formation law (Kennicutt, 1998; Schmidt, 1959), where

$$\Sigma_{\rm SFR} \propto \Sigma^{1.4}. \tag{4.6}$$

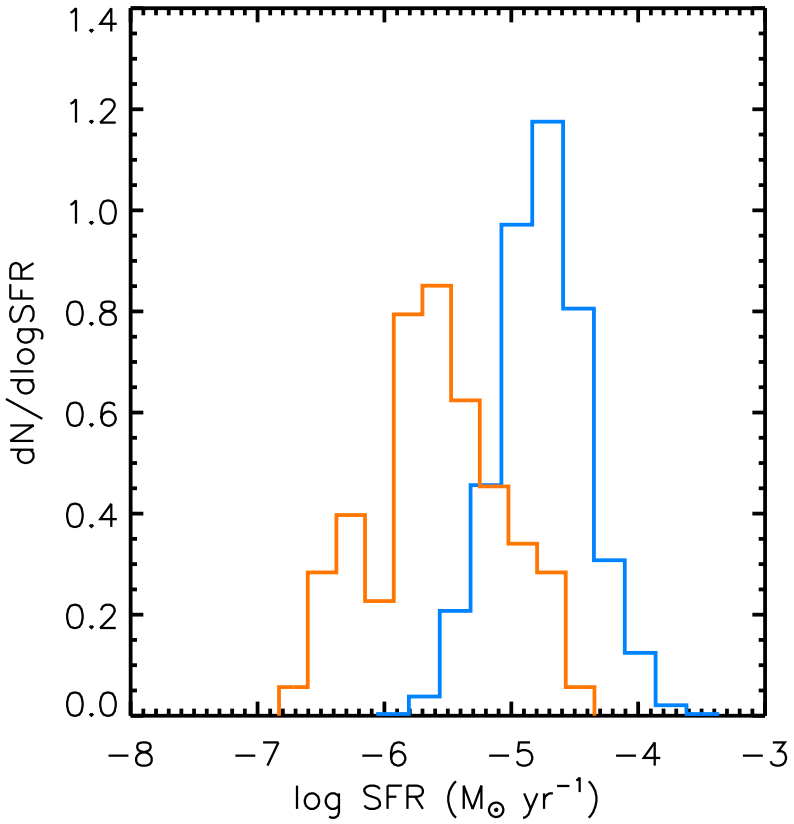

Figure 4.6 – Distributions for the star formation rate (SFR) of our inner disc (blue histogram) and outer disc (orange histogram) molecular clouds at 500 Myr. The inner and outer disc are divided at 8 kpc (see text). The distributions are normalized by the number of clouds and by the bin size.

Bigiel et al. (2008) studied the inner discs of several nearby galaxies and found that $\Sigma_{\rm SFR}$ was more closely correlated with the molecular H_2 surface density than with the HI or total gas surface densities. However, after studying the outer discs of nearby galaxies and finding a strong trend between the HI surface density and the SFR, Bigiel et al. (2010a) concluded that the HI surface density profile was a key environmental factor causing inefficient star formation in the outer discs of galaxies. We find that our simulated disc has less efficient star

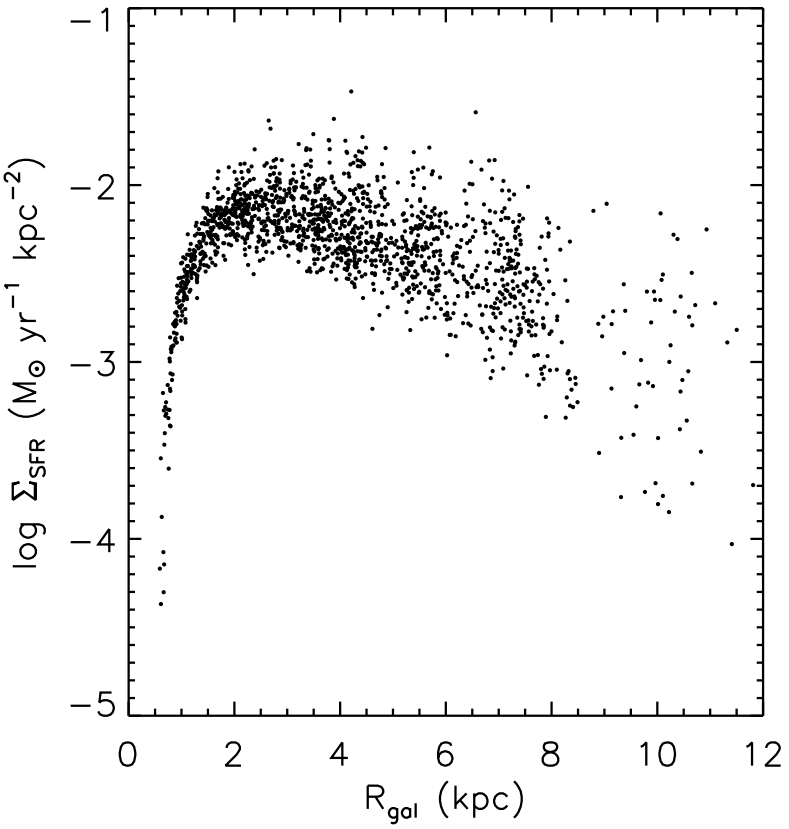

Figure 4.7 – Star formation rate surface density ($\Sigma_{\rm SFR}$) as a function of the galactocentric radius for molecular clouds in our sample at 500 Myr. Note the similar shape to the shear-supported boundary for the Toomre mass in Figure 4.5.

formation in its outer disc due to the shape of the surface density profile as it decreases with galactocentric radii, consistent with the findings of Bigiel et al. (2010a).

4.4 Summary and Discussion

We simulated a large-scale galactic disc to explore the effects of environment on the structure of molecular clouds. We found that a substantial population of unbound clouds formed naturally in a galactic disc environment. We found that the distributions of properties for our clouds were consistent with those measured in observations of M33 by Rosolowsky et al. (2007). We also showed that our cloud sizes, masses, and velocity dispersions satisfied the Larson scaling relations, confirming the presence of these relations in clouds at extragalactic distances on global size scales. We conclude that a mixed population of bound and unbound clouds formed in a galactic disc under the influence of turbulence, gravity, galactic potential, shear, stellar feedback, and external pressure can match observations when studied in an extragalactic context.

By separating our clouds into two populations based on their location in the disc, we explored their properties in the context of their environment. Using Toomre analysis, we found galactic shear to be an important environmental factor affecting the upper limit of cloud properties in the outer disc, particularly due to a narrowing envelope of instability at large radii caused by a decrease in the timescales for collapse. This narrowing produces a lower Toomre mass for fragmentation than in the inner disc, resulting in smaller, lower mass clouds in the outer disc. We also explored the effect of environment on stars and found that the SFR decreases with increasing galactocentric radius. Since lower HI column densities are common in the outer discs of nearby galaxies (Bigiel et al., 2010a) and we find lower cloud surface densities in the outer disc of our simulated galaxy, we conclude that one of the most important factors

for the SFR is the underlying surface density profile of the disc, consistent with observations and the Kennicutt-Schmidt star formation relation.

To understand the role of external pressure on our clouds, we consider the results of Leroy et al. (2015) who used the v_o-Σ relation to determine whether the clouds in their sample are in virial equilibrium or require pressure confinement to explain their high linewidths. These authors showed that clouds in the Galactic centre (Oka et al., 2001) and the outer Milky Way (Heyer, Carpenter, & Snell, 2001) have high size-linewidth coefficients which can be understood as a reflection of the pressure in the surrounding medium. While some clouds can be explained with reasonable external pressures, others would require pressures $P/k_{\rm B} > 10^7$ cm^{-3} K, several decades greater than the typical pressures in the ISM. Therefore, many of these clouds may be gravitationally unbound. Although we find in our v_o-Σ relation shown in Figure 4.3 that ~ 70 % of our clouds are gravitationally bound with $\alpha < 2$ and do not require any pressure confinement, those with $\alpha > 2$ could be explained with $P/k_{\rm B} > 10^{4-5}$ cm^{-3} K, consistent with the thermal pressure throughout the disc (Benincasa et al. 2015, in preparation). However, the importance of galactic shear in the disc and the effect of the total angular momentum of the clouds on α and the retrograde population from cloud interactions leads us to conclude that these clouds are in fact unbound. Also, although we do not find a correlation between the SFR and the virial parameter, we have seen indications that those with the highest SFRs are gravitationally bound, prograde clouds with low axial tilts and $1 < \alpha < 2$. We will explore this further in future work to determine the role of the virial parameter and whether or not the SFR can be strongly linked to the boundedness of molecular clouds.

4.5 Acknowledgments

The authors thank SHARCNET (Shared Hierarchical Academic Research Computing Network), SciNet, and Compute/Calcul Canada, who provided dedicated resources to run these simulations. This work was supported by NSERC.

Bibliography

Agertz, O., Kravtsov, A. V., Leitner, S. N., & Gnedin, N. Y. 2013, ApJ, 770, 25

Ballesteros-Paredes, J., Vázquez-Semadeni, E., Gazol, A., et al. 2011, MNRAS, 416, 1436

Benincasa, S. M. et al. 2015, in preparation

Bertoldi F. & McKee C. F. 1992, ApJ, 395, 140

Bigiel, F., Leroy, A., Walter, F., et al. 2008, AJ, 136, 2846

Bigiel, F., Leroy, A., Walter, F., et al. 2010a, AJ, 140, 1194

Bigiel, F., Bolatto, A. D., Leroy, A. K., et al. 2010b, ApJ, 725, 1159

Binney, J. & Tremaine, S. 2008, Galactic Dynamics, 2nd Ed. (Princeton University Press)

Bolatto, A. D., Leroy, A. K., Rosolowsky, E., Walter, F., & Blitz, L. 2008, ApJ, 686, 948

Bonnell, I. A., Smith, R. J., Clark, P. C., & Bate, M. R. 2011, MNRAS, 410, 2339

Brand, J., & Wouterloot, J. G. A. 1995, A&A, 303, 851

Clark, P. C., Bonnell, I. A., Zinnecker, H., & Bate, M. R. 2005, MNRAS, 359, 809

Clark, P. C., Bonnell, I. A., & Klessen, R. S. 2008, MNRAS, 386, 3

Corbelli, E., & Salucci, P. 2000, MNRAS, 311, 441

Dobbs, C. L., Burkert, A., & Pringle, J. E. 2011a, MNRAS, 413, 2935

Dobbs, C. L., Burkert, A., & Pringle, J. E. 2011b, MNRAS, 417, 1318

Dobbs, C. L., Krumholz, M. R., Ballesteros-Paredes, J., et al. 2014, Protostars and Planets VI, 3

Field, G. B., Blackman, E. G., & Keto, E. R. 2011, MNRAS, 416, 710

Freedman, W. L., Wilson, C. D., & Madore, B. F. 1991, ApJ, 372, 455

Governato, F., Willman, B., Mayer, L., et al. 2007, MNRAS, 374, 1479

Heyer, M. H., Carpenter, J. M., & Snell, R. L. 2001, ApJ, 551, 852

Heyer, M. H., Corbelli, E., Schneider, S. E., & Young, J. S. 2004, ApJ, 602, 723

Heyer, M., Krawczyk, C., Duval, J., & Jackson, J. M. 2009, ApJ, 699, 1092

Hopkins, P. F., Quataert, E., & Murray, N. 2012, MNRAS, 421, 3488

Hughes, A., Meidt, S. E., Colombo, D., et al. 2013, ApJ, 779, 46

Keller, B. W., Wadsley, J., Benincasa, S. M., & Couchman, H. M. P. 2014, MNRAS, 442, 3013

Kennicutt, R. C., Jr. 1998, ApJ, 498, 541

Lada, C. J., & Lada, E. A. 2003, ARA&A, 41, 57

Larson, R. B. 1981, MNRAS, 194, 809

Leroy, A. K., Bolatto, A. D., Ostriker, E. C., et al. 2015, ApJ, 801, 25

Lombardi, M., Alves, J., & Lada, C. J. 2010, A&A, 519, 7

Monaghan, J. J., & Lattanzio, J. C. 1985, A&A, 149, 135

Murray, N. 2011, ApJ, 729, 133

Oka, T., Hasegawa, T., Sato, F., Tsuboi, M., Miyazaki, A., & Sugimoto, M. 2001, ApJ, 562, 348

Robitaille, T. P., & Whitney, B. A. 2010, ApJL, 710, L11

Rosolowsky, E., Engargiola, G., Plambeck, R., & Blitz, L. 2003, ApJ, 599, 258

Rosolowsky, E., Keto, E., Matsushita, S., & Willner, S. P. 2007, ApJ, 661, 830

Schinnerer, E., Meidt, S. E., Pety, J., et al. 2013, ApJ, 779, 42

Schmidt, M. 1959, ApJ, 129, 243

Stinson, G., Seth, A., Katz, N., et al. 2006, MNRAS, 373, 1074

Tasker, E. J., & Bryan, G. L. 2008, ApJ, 673, 810

Tasker, E. J. & Tan, J. C. 2009, ApJ, 700, 358

Tasker, E. J. 2011, ApJ, 730, 11

Toomre, A. 1964, ApJ, 139, 1217

Wadsley, J. W., Stadel, J., & Quinn, T. 2004, New Astronomy, 9, 137

Ward, R. L., Wadsley, J., Sills, A., & Petitclerc, N. 2012, ApJ, 756, 119

Ward, R. L., Wadsley, J., & Sills, A. 2014, MNRAS, 439, 651

Williams, J. P., de Geus, E. J., & Blitz, L. 1994, ApJ, 428, 693

Wolfire, M. G., McKee, C. F., Hollenbach, D., & Tielens, A. G. G. M. 2003, ApJ, 587, 278

Chapter 5

Conclusion and Future Work

This thesis began with the question: what would the impact on star formation be if some molecular clouds are gravitationally unbound? We explored the dynamics, structural properties, evolution, and formation of unbound molecular clouds using isolated and galactic disc simulations. The goal of this thesis was to determine whether a mixed population of bound and unbound star-forming clouds could match observations of local molecular clouds as well as those in nearby galaxies. By studying simulated unbound clouds in an observational context, we aimed to challenge the commonly-held view that molecular clouds must be in virial equilibrium to form stars and remain consistent with observations.

In Chapter 2, we explored whether a mixed population of bound and unbound clouds could reasonably match the observed relation between the size-linewidth coefficient, $v_{\rm o} = \sigma_{\rm v}/R^{1/2}$, and the surface density, Σ, as seen in observations by Heyer et al. (2009). Using a sample of simulated molecular clouds, we reproduced the observed relation and showed that such a spread in the intrinsic virial parameter naturally produces the scatter in the size-

linewidth coefficient for a given surface density, supporting the presence of a substantial population of unbound clouds. This chapter demonstrated that a mixed population of bound and unbound star-forming clouds can accurately match the observed scaling relation and accompanying scatter of Heyer et al. (2009) for nearby low-mass clouds in the Milky Way.

We continued our exploration of the observable properties of our sample of simulated molecular clouds in Chapter 3 by analysing the evolution of cloud structure as characterised by the probability distribution function (PDF) of the mass surface density. We showed that, regardless of their boundedness, the mass surface density PDFs for our clouds had lognormal distributions which developed power-law tails at late times, consistent with recent observations (e.g. Kainulainen et al., 2009; Schneider et al., 2015) and model predictions (e.g. Ostriker et al., 2001; Tassis et al., 2010). Since the peak of the PDF crosses the observational detection threshold, a power-law is the most suitable descriptor of structure in the observable regime: a conclusion which is supported by recent observations of nearby molecular clouds by Lombardi et al. (2014, 2015). This chapter provides further evidence that a mixed population of bound and unbound molecular clouds can match observations – in this case, the mass surface density PDFs probing structure of local clouds – based on synthetic observations of clouds formed in isolation.

In Chapter 4, we used a large-scale galactic disc simulation to show that a mixed population of bound and unbound clouds forms naturally in a galactic disc environment, exposed to the effects of the galactic potential, shear, stellar feedback, and external pressure from the surrounding ISM. We found that this sample of clouds exhibits similar scaling relations to those seen for the

simulated low-mass isolated clouds studied in Chapters 2 and 3. We also showed that the clouds in the outer disc are less massive and have lower, more inefficient star formation rates than those in the inner disc due to the overall gas surface density profile, consistent with recent observations of M33 (Bigiel et al., 2010) and the Kennicutt-Schmidt star formation law. The conclusions of Chapter 4 solidify our previous results in Chapters 2 and 3 and support our hypothesis by demonstrating that a mixed population of bound and unbound clouds forms naturally and can suitably match observations when studied in an extragalactic context.

This thesis demonstrates that not only can our understanding of recent observations of Galactic and extragalactic molecular clouds benefit from the presence of unbound clouds, but their existence is a natural consequence of cloud formation and evolution in the galaxy.

5.1 Broader Implications of a Population of Unbound Clouds

The results of this thesis have profound implications on several fundamental aspects of star formation and the evolution of galactic structure. Despite how extensively molecular clouds have been studied in galactic and extragalactic observations and simulations, their formation, dynamics, structure, and evolution are not very well understood. Molecular cloud dynamics have long been characterised by "Larson's laws," empirical scaling relations between the mass, size, and velocity dispersion, which showed that molecular clouds are gravitationally bound and in virial equilibrium (Larson, 1981). However, recent observations showed that this interpretation may be the result of ob-

servational bias from probing a narrow range of surface densities. Our work confirms that Larson's laws are not sufficient at describing the structure and dynamics of molecular clouds unless clouds are probed over a narrow range of surface densities with an explicit assumption of virial equilibrium. In a space defined by the size-linewidth coefficient, surface density, and virial parameter, Larson's size-linewidth relation would be represented by a single point (constant surface density and virialised, $\alpha = 1$). We showed that observed properties of molecular clouds can be understood if clouds fully populate a two-dimensional space parameterised by the surface density and virial parameter, with a slight preference for being unbound. By removing this limitation that molecular clouds must be in virial equilibrium, several long-standing issues regarding star formation and galactic structure and evolution can be resolved.

One such issue is the low galactic star formation rate observed for the Milky Way and other nearby galaxies (e.g. Krumholz & Tan, 2007). Our work shows that the low star formation rates and efficiencies can be explained by a substantial role for unbound clouds. Molecular clouds which are gravitationally unbound would naturally lead to inefficient star formation due to only a small fraction of the molecular gas participating in localised collapse. As these localised regions, formed by turbulence, collapse into star-forming cores, the remaining gas would disperse gradually, fading below the limit of detection into the background ISM, as we saw in Chapter 3.

Another long-standing issue is whether molecular clouds are long- or short-lived objects. A population of unbound clouds would be very transient, as they would be readily disrupted by various forms of stellar feedback and cloud-

cloud collisions (Dobbs et al., 2011). The formation timescale estimated from our Toomre analysis of the disc in Chapter 4 is approximately 13 ± 3 Myr, which is consistent with recent estimates of cloud lifetimes (Murray, 2011), demonstrating that the formation of molecular clouds is in rough equilibrium with their destruction in a galactic disc. Our results therefore support the short-lived, rather than the long-lived, nature of clouds.

We also offer a means of determining cloud age during the earliest phase of star formation based on the evolving slope of the power-law tail of the surface density PDF. The power-law tails in our PDFs have slopes and deviation points which each approach constant values with time. This result suggests that the surface density PDF of molecular clouds is a direct precursor to the stellar initial mass function (IMF) – the near-universal initial distribution of stellar masses found in many star-forming environments – which also has a lognormal shape and a high-mass power-law tail with a constant slope. Establishing a relationship between the underlying gas structure and distribution of stars and stellar clusters can lead us towards a greater understanding of the origin and universality of the stellar IMF.

5.2 Future Directions

Star formation is a hierarchical process, which is influenced by the structure and dynamics of the host molecular clouds and surrounding ISM. This hierarchy poses a challenge for simulators and observers, as the processes involved in star formation occur at different size scales spanning many orders of magnitude. Recent efforts by simulators (e.g. Rey-Raposo et al., 2015; Dobbs, 2015; Bonnell et al., 2013) to overcome this issue have involved extracting

clouds from large-scale galactic disc simulations and re-simulating the clouds with and without gravity at higher resolution. The outcome is that the higher resolution runs capture the internal structure of the molecular clouds while retaining the history of having lived in a galactic disc environment; however, this method can be very imprecise due to the many assumptions made during the extraction and re-simulation process. In future work, we aim to avoid the uncertainties stemming from this method by taking a known entity – our isolated simulation of the turbulent ISM (see Chapter 2) – and placing it in the highly-resolved annulus of a simulated galactic disc. Using the same initial conditions would allow us to explore the detailed structure and dynamics of a cloud previously studied in isolation and determine the direct impact of galactic shear, galactic potential, and the external pressure from the surrounding ISM on its properties. In this study, we would also have high enough resolution to be able to definitively determine whether the star formation rate and also the cluster mass can be strongly linked to the boundedness of molecular clouds.

Another possible direction would be to explore the effects of radiative transfer on our simulations of bound and unbound star-forming molecular clouds. Due to the new efficient implementation of radiative transfer in GASOLINE by Woods et al. (in prep), we can now study the evolution of star-forming and cluster-forming cores in detail. Our current simulations of isolated clouds are entirely isothermal as they explore the earliest stages of star formation when the gas can still be approximated as optically thin; however, at later stages once the compact young stellar objects begin to form within the dense cores and gas exceeds the opacity limit for fragmentation, the gas becomes optically

thick and radiative transfer from the newly-luminous protostars becomes important. A study including radiative transfer would also allow us to explore cloud lifetimes in greater detail through the eventual disruption and dispersal of bound and unbound molecular clouds.

Molecular clouds found in the cold, dark "empty space" between stars are endlessly curious objects. As the structures shaping the morphology of our Galaxy and the principal sites of star and planet formation, understanding the true nature of these clouds is crucial in order to obtain a better picture of galaxy evolution and the origins of stars and life in the Universe. By bridging the gap between stars and galaxies, between large scales and small scales, and between observations and simulations, this thesis has demonstrated that molecular clouds that are highly transient and unbound can form naturally, are supported by recent observations, and can help explain several open questions in astrophysics. These important results open up a new paradigm for understanding star formation and the structure and evolution of the Galaxy in the context of unbound molecular clouds.

Bibliography

Bigiel, F., Leroy, A., Walter, F., Blitz, L., Brinks, E., de Blok, W. J. G., & Madore, B. 2010, AJ, 140, 1194

Bonnell, I. A., Dobbs, C. L., & Smith, R. J. 2013, MNRAS, 430, 1790

Dobbs, C. L., Burkert, A., & Pringle, J. E. 2011, MNRAS, 413, 2935

Dobbs, C. L. 2015, MNRAS, 447, 3390

Heyer, M., Krawczyk, C., Duval, J., & Jackson, J. M. 2009, ApJ, 699, 1092

Kainulainen, J., Lada, C. J., Rathborne, J. M., & Alves, J. F. 2009, A&A, 497, 399

Krumholz, M. R., & Tan, J. C. 2007, ApJ, 654, 304

Larson, R. B. 1981, MNRAS, 194, 809

Lombardi, M., Bouy, H., Alves, J., & Lada, C. J. 2014, A&A, 566, A45

Lombardi, M., Alves, J., & Lada, C. J. 2015, A&A, 576, L1

Murray, N. 2011, ApJ, 729, 133

Ostriker, E. C., Stone, J. M., & Gammie, C. F. 2001, ApJ, 546, 980

Rey-Raposo, R., Dobbs, C., & Duarte-Cabral, A. 2015, MNRAS, 446, L46

Salim, D. M., Federrath, C., & Kewley, L. J. 2015, arXiv:1505.03144

Schneider, N., Ossenkopf, V., Csengeri, T., et al. 2015, A&A, 575, A79

Tassis, K., Christie, D. A., Urban, A., et al. 2010, MNRAS, 408, 1089

Woods, R. M. et al. 2015, in preparation